2013

Surface Enhanced Raman Scattering and Fluorescence of Tagged Phospholipids in Langmuir-Blodgett Monolayers

Aisha Abdulwahab Alsaleh
University of Windsor

Surface enhanced Raman scattering and fluorescence of tagged phospholipids in Langmuir-Blodgett monolayers

By

Aisha Abdulwahab Alsaleh

A Thesis

Submitted to the Faculty of Graduate Studies

through Chemistry and Biochemistry

in Partial Fulfillment of the Requirements for

the Degree of Master of Science at the

University of Windsor

Windsor, Ontario, Canada

2013

Surface enhanced Raman scattering and fluorescence of tagged phospholipids in Langmuir-Blodgett monolayers

By

Aisha Abdulwahab Alsaleh

APPROVED BY:

_____

D. Northwood

Mechanical, Automotive & Materials Engineering

_____

H. Eichhorn

Department of Chemistry & Biochemistry

_____

R. Aroca

Department of Chemistry & Biochemistry

September 27, 2013

DECLARATION OF CO-AUTHORSHIP / PREVIOUS PUBLICATION

I. Co-Authorship Declaration

By this means, I announce in general that this thesis combines result of joint research, as follow:

This thesis combines the result of Co-operation work with Diogo Volpati**,** Carlos J. L. Constantino, under supervision Dr. Ricardo F. Aroca. The collaboration is presented in chapter 4 and 5 of this thesis. In all cases, the key ideas, primary contributions, the author performed experimental designs data analysis and interpretation.

I am aware of the University of Windsor Senate Policy on Authorship and I certify that I have properly acknowledged the contribution of other researchers to my thesis, and have obtained written permission from each of the co-author(s) to include the above material(s) in my thesis.

I certify that, with the above qualification, this thesis, and the research to which it refers, is the product of my own work

II. Declaration of Previous Publication

This thesis includes one original paper that is currently in press in John Wiley and Sons, as follows:

Thesis Chapter	Publication title/full citation	Publication status
Chapter 4 and 5	Plasmon enhanced scattering and fluorescence used for ultrasensitive detection in Langmuir-Blodgett monolayers	In press

I certify that I have obtained a written permission from the copyright owner(s) to include the above-published material in my thesis. I certify that the above material describes work completed during my registration as graduate student at the University of Windsor.

I declare that, to the best of my knowledge, my thesis does not infringe upon anyone's copyright nor violate any proprietary rights and that any ideas, techniques, quotations, or any other material from the work of other people included in my thesis, published or otherwise, are fully acknowledged in accordance with the standard referencing practices. Furthermore, to the extent that I have included copyrighted material that surpasses the bounds of fair dealing within the meaning of the Canada Copyright Act, I certify that I have obtained a written permission from the copyright owner(s) to include such material(s) in my thesis.

I declare that this is a true copy of my thesis, including any final revisions, as approved by my thesis committee and the Graduate Studies office, and that this thesis has not been submitted for a higher degree to any other University or Institution.

ABSTRACT

The surface-enhanced Raman scattering (SERS) and surface-enhanced resonance Raman scattering (SERRS) phenomena can be observed when molecules are close to metallic nanoparticles that sustain localized surface plasmon resonances (LSPR). There is a broad spectrum of metallic nanostructures (mainly silver and gold) that may be used to improve the efficiency of Raman signals. Here, we used silver island films (SIFs) to enhance the scattering from tagged phospholipids coating the SIFs, and fabricated using Langmuir-Blodgett (LB) technique. Single molecule detection (SMD) can be approached using LB-SERRS technique and using mixed LB monolayer, containing about one target molecule per 1 μm^2 of surface area.

Fluorescence enhancement is achieved with shell-isolated nanoparticles (SHINs) synthesized and delivered to the LB substrate, a technique we term SHINEF. Simply, a drop of SHINs is delivered to quartz slide covered by LB of tag-phospholipid to produce surface-enhanced florescence.

For my father, Abdulwahab Alsaleh, RIP

ACKNOWLEDGEMENTS

I was pleased and honoured to have been oversaw the completion of this thesis and I would like to thank Professor Dr. Aroca Ricardo for his care and efforts, without his guidance and continued assistance this thesis would not have been possible.

I would like to thank my committee members, Dr. Holger Eichhorn and Dr. Derek Northwood for their giving time and helpful suggestions.

I also acknowledge Chemistry and Biochemistry Department for support and excellent research environment. I extend a heartfelt thank you to Marlene Bezaire for all your help and support. Acknowledgement is due to the Saudi Arabian Cultural Bureau in Canada for the financial support.

I would also like to thank the MSSG Members in Lab B-77: Ariel, Haider, Diogo, Gabriel, Kate, Igor, I could not complete my work without their friendship and assistance. I wish to thank my best friends Dhuha and Miaad for all the emotional support and entertainment they provided.

Special thanks for my father Abdulwahab, who left us too soon, and my mother Qumash, I own them for them love, raised, support and encouragement, I would not be the person I am today without you. I wish this work make you proud. I extend my thanks and heartfelt love to my brother: Saleh and my sisters: Mwaheb, Safa, Marwah, Mona and my little sister monerah who have been with me all the time to spur my morale. My full gratitude to my mother in law: Husa for her deep prayer and support.

Above all, I would like to thank my husband Abdulrauf and my daughter Wasan for the personal support and great patience at all times.

Table of Contents

LIST OF TABLES

LIST OF FIGURES

LIST OF ABBREVIATIONS

AA	Arachidic Acid
AFM	Atomic Force Microscopy
APTMS	3-aminopropyltrimethoxysilane
BSE	Back Scattering Electrons
CARS	Coherent anti-Stokes Raman scattering
CCD	Charged Coupled Device
DNA	Deoxyribonucleic acid
EBSD	The diffracted backscattered electrons
EDS	Energy-dispersive X-ray spectroscopy
EF	Enhancement Factor
EM	Electromagnetic
FCS	Fluorescence correlation spectroscopy
F-DHPE	*N*- (Fluorescein-5-Thiocarbamoyl)-1,2-Dihexadecanoyl-*sn*-Glycero-3-Phosphoethanolamine, Triethylammonium Salt
FTIR	Fourier transform infrared spectroscopy
LB	Langmuir-Blodgett
LbL	Layer-by-LAYER
LL	Laser Line
LSPR	Localized Surface Plasmon Resonance
MEF	Metal Enhanced Fluorescence
NP	Nanoparticle
R18	Octadecyl Rhodamine B chloride
RRS	Resonance Raman Scattering
RS	Raman Scattering
SE	Secondary Electron
SERRS	Surface Enhanced resonance Raman Scattering
SERS	Surface Enhanced Raman Scattering
SEF	Surface-enhanced Fluorescence
SEM	Scanning Electron Microscopy
SHIN	Shell Isolated Nanoparticle
SHINEF	Shell Isolated Nanoparticles-Enhanced Fluorescence
SHINERS	Shell Isolated Nanoparticles-Enhanced Raman Scattering
SMD	Single Molecule Detection
SPM	Scanning probe microscopes
TERS	Tip-enhanced Raman spectroscopy
TEM	Transmission Electron Microscopy
UV-Vis	Ultraviolet-Visible

Chapter 1

INTRODUCTION

1.1 Introduction

The interaction of electromagnetic radiation or light with matter leads to a wide range of optical processes. Here we deal with a very narrow field where the electromagnetic radiation is in the ultraviolet-visible range and molecules that absorb light in the visible range. The linear optical processes we consider are then the absorption, the emission and the inelastic scattering of light or the Raman effect[1-3]. The main focus of the work is on the amplification of fluorescence emission and Raman scattering using gold and silver nanostructures[4, 5].

Raman spectroscopy is a widely used spectroscopic technique in material science[6]. It gives specific molecular structure fingerprints through the measuring of inelastic light scattering that is related to molecular vibration[7]. However, the Raman cross-section is about 10^{-29} cm^2 per molecule, in the common case when there is no resonance excitation; but fluorescence could be as high as 10^{-17} cm^2 per molecule [8, 9]. Surface-enhanced spectroscopy (SES) is based on the used of plasmonics[10] to enhanced optical signals, in particular; surface enhanced Raman scattering (SERS) and surface enhanced fluorescence (SEF)[11, 12].

Surface enhanced Raman scattering provides signal amplifications for incident light far from resonance with an internal molecular electronic state (NR-normal Raman effect). Surface enhanced Resonance Raman scattering (SERRS), on the other hand, is achieved when the laser excitation frequency is in resonance with a molecular electronic state[13]. The plasmon enhancement or electromagnetic (EM) enhancement[14, 15] is attained mainly with nanostructures of gold, silver, and copper with an average enhancement factor (EF) of ca. 10^6 when performing routine SERS experiments. The

molecular-plasmon coupling is essential for the amplification of signals in this type of spectroscopy[16]. Therefore, good control of shape, space between nanoparticles, dielectric environment, and functionalization of nanoparticles are important in obtaining optimized SERS[17].

SERS and, in particular, SERRS allow for single molecule detection (SMD)[18, 19]. On the other hand, the high cross section of fluorescence is an important consideration in the application of SMD, that has grown over the years and it is finding applications in cell signalling, enzyme reactions, protein dynamics, molecular motors, and sequencing of DNA[20]. Raman vibrational spectra have vibrational fingerprints, which help to show the molecules' structural information. With the use of SERRS molecular and plasmon resonance conditions are easily fulfilled, and thus make it very easy when detecting single molecules. Preparation of substrates that are SERS- active poses great challenge because of their non-uniformity in their activity.

Using SERRS/SERS in detection of single molecules was found to be only possible in gold or silver nanoparticles at sites of the greatest enhancement, this highly concentrated EM fields are called hot spots[21]. In our group, the Langmuir-Blodgett (LB) approach is used to control the target molecules within a single monolayer, for their detection via SERRS/ SERS or SEF. Fabrication of enhancing structures is faced with a number of challenges, which makes difficult to correlate SERS signals to specific hot spots [22]. In addition, there are several complexities that may arise in SERS, which include; interaction of nanostructure with the molecule to be tested, photoreactions induced by electromagnetic incident radiation. [23]

Efforts have been made in chapter 2 to cover fundamental elements of Raman scattering and fluorescence phenomena, the enhancement fluorescence in localized

surface Plasmon resonance (LSPR) through the use of a dipolar model and the origin of surface enhanced Raman scattering (SERS) and surface enhanced resonance Raman scattering (SERRS). Discussion of mechanisms used in PEF enhancement will also be covered and the introduction of shell-isolated nanoparticle (SHIN).

Chapter 3 reviews the instruments used in this work. The preparation of Ag island films by vacuum evaporation technique and the Langmuir-Blodgett (LB) technique are discussed. The characterization using UV-Vis absorption spectroscopy and Raman and fluorescence spectroscopy is described. Also the morphological techniques including atomic force microscopy (AFM) and scanning electron microscopy (SEM) are presented. The synthesis of Au and Ag SHINs is given.

In chapter 4, we describe the method of preparation of SHINEF active substrate by using a surface silanization technique, and deposit Ag SHINs by self-assembly with different period of time to control the surface coverage. The LB technique is used to coat the substrates with Rhodamine B dye.

Chapter 5 presents the averaged LB-SERRS of tag-phospholipid, and characteristics are discussed. Also the fluorescence spectrum using Au SHINs is presented. Therefore the plasmon enhancement of the tag-phospholipid fluorescence can be measured.

In chapter 6, we extend the work to a tagged phospholipid commonly used in bio-spectroscopy to demonstrate the feasibility of enhanced fluorescence (SHINEF), and also surface-enhanced resonance Raman scattering (SERRS) on SIF.

Finally, chapter 7 contains the conclusions of this work and the future work.

Chapter 2

BACKGROUND

2.1 Introduction

Within the Born-Oppenheimer approximation, the molecular energy levels can be classified as: electronic, vibrational and rotational states[1]. The interaction of a molecule with electromagnetic (EM) radiation may lead to absorption or scattering of EM radiation. The high energy electronic states lead to absorption of EM radiation in the ultraviolet and visible spectral region (UV-visible spectroscopy)[2]. Vibrational energy levels may absorb light in the infrared region of the EM spectrum[7]. Rotational energy levels are detected in the microwave region, or in the fine structure of the vibrational or electronic spectra. Under standard conditions of pressure and temperature most molecules are found in their ground electronic state, and also in their ground vibrational state. The population of vibrational states, as a function of temperature, is easily explained by the Boltzmann distribution function[1]. In this work, we focus on the emission of EM radiation, in particular fluorescence[24], and the inelastic scattering of EM radiation , or Raman scattering; and the amplification of these optical signals using metallic nanostructures[4, 5].

2.2 Emission and scattering

When a material interacts with monochromatic light of wavenumber ω_0, apart from the fact that most of the incident light may be transmitted without change, a fraction of it is either absorbed or scattered. Spectral analysis of the scattered light shows that, in addition to scattering without change of wavenumber of the incident light (Rayleigh scattering), one photon in ten millions of photons is detected with a different wavenumber (Raman scattering). In practise, pairs of new Raman lines are observed in the spectrum at

wavenumbers to be found symmetrically with respect to the unchanged Rayleigh line[3, 6]. The observed wavenumber differences correspond to transitions between vibrational (and rotational) energy levels of the molecule. This inelastic scattering of light is known as *Raman effect* or *Raman scattering[3]*. A molecule must have polarizability to Raman scatter also it is symmetry must be even to have this polarizability. Using classical theory, the magnitude of the induced electric dipole p is proportional to the magnitude of the polarizability as well as the incident electric field E, expressed by this equation:

$$p = \alpha E \qquad [2.1]$$

Polarizability is a measured of particles response to the outside eclectic field and represents the molecular electronic cloud volume. When an incident radiation at frequency near the frequency of the electronic transition of he molecule a resonance will occur. This provides enough energy to excite the electrons to the higher energy state, achieving Resonance Raman Scattering (RRS).

Absorption of light may lead to fluorescence (and/or phosphorescence), a photon emission process that occurs during molecular relaxation from the lowest electronic excited state[24]. Fluorescence involves transitions between electronic and vibrational states of polyatomic molecules (fluorophores). The Jablonski diagram[25] (Figure 2.1) offers a convenient representation of the excited state structure and the relevant transitions. Each electronic state contains multiple sublevels representing the vibrational modes of the molecule. Since electronic energies are much higher than vibrational energies, light with energies in the ultraviolet to the blue-green region of the spectrum are needed to trigger an electronic transition. Under standard conditions, a molecule, predominantly resides in the electronic ground state. The main parameters of

experimentally measured fluorescence are: the radiative decay, the non-radiative decay and the quantum yield measure at a particular set of experimental conditions[26].

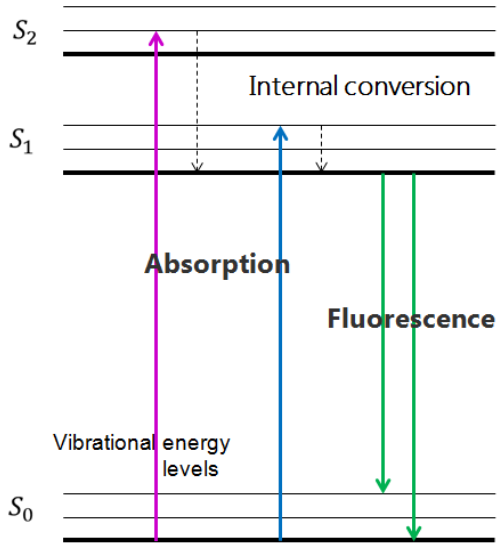

Figure 2.1 Jablonski diagram

(Jablonski, A., *Über den Mechanisms des Photolumineszenz von Farbstoffphosphoren.* Z. Phys., 1935. 94: p. 38-46)

The Quantum Yield defines the efficiency of the entire fluorescence emission process. Quantum yield is described as the ration of photons emitted and absorbed and is calculated with following formula.

$$Q = \frac{number\ of\ emitted\ \text{photons}}{number\ of\ \text{absorbed photons}} \qquad [2.2]$$

The quantum yield is also given in terms of the radiative Γ_{rad} and non-radiative decay ratesΓ_{nR}:

$$Q = \frac{\Gamma_{rad}}{\Gamma_{rad}+\Gamma_{nR}} \qquad [2.3]$$

In case of 100% efficiency, the Quantum yield will be 1.0 i.e. each and every photon that was absorbed by the substance will be emitted.

Fluorescence is an efficient process compared to inelastic scattering of the Raman effect. For high quantum yield fluorophores the optical cross section can be of the order of 10^{-17} cm^2, while normal Raman scattering cross section are ca. 10^{-29} cm^2 [4, 5]. The discovery of surface enhanced Raman scattering[11] and its plasmonic origin[12, 27], brought to the forefront the role of certain metallic nanoparticles in the enhancement of optical signals. This new analytical technique may enhance the optical cross sections by several orders of magnitude. In the case of Raman scattering enhancement factor of 10^{10} or even higher have been reported allowing the detection of a single molecule[18, 19]. The fluorescence enhancement is much modest; but the enhancement of an already strong optical signal is significant for many applications. In this work we investigate the scattering and fluorescence enhancement in tag-phospholipids using silver and gold nanostructures. The plasmonic origin of the enhancement requires the presence of nanostructures that can sustain localized surface plasmon resonances (LSPR).[10] Metallic nanoparticles, in particular silver and gold, can strongly scatter and absorb incident light through localized surface plasmon resonances. For particles whose sizes are small compared to the incident wavelength, a simple quasi-static point dipole approximation can be employed to describe their interaction with light. The physical interaction with light of small and large nanoparticles can be best described using Mie scattering theory[28], allowing the computation of scattering and absorption cross-sections which can be much larger than their geometrical sizes. For example, the absorption cross section of Rhodamine 6G is $10^{-16} cm^2$.

Therefore: $10^{-16}\ cm^2 = 10^{-2} nm^2 = 1 A^{\circ 2}$. However, the cross section for the absorption (or scattering) of a 40 nm diameter silver sphere is about $10^{-10}\ cm^2 = 10^4 nm^2$, that

corresponds to a geometrical size of 56 nm in diameter. Absorption and scattering cross sections solution are shown below, respectively:

$$\sigma_{abs} = 4ka^3 Im\left[\frac{\varepsilon-\varepsilon_m}{\varepsilon+2\varepsilon_m}\right] \qquad [2.4]$$

$$\sigma_{sca} = \frac{8\pi}{3} k^4 a^6 \left[\frac{\varepsilon-\varepsilon_m}{\varepsilon+2\varepsilon_m}\right]^2 \qquad [2.5]$$

Where k equals to $\frac{2\pi}{\lambda}$, a is the Radius of the sphere, ε is the Dielectric constant of the spherical particle and ε_m is the Dielectric constant of the medium.

Plasmon resonances of the two nanoparticles can coupled together leading to new resonances and amplified near electric fields as recently shown for silver island films (SIF)[29]. The results of the latter work are important for the present applications, since we also use SIF for SERS and surface enhanced resonance Raman of tag-phospholipids. The properties of the coupling and the effect on the plasmon resonances are illustrated in Figure 2.2 taken from reference[29]. The results of computations shown in Figure 2.2 help to understand the observation of red shifted plasmons in SIF fabricated by vacuum evaporation on glass substrates, where the best model is that of hemispherical dimers. The hemispherical dimers provide a plasmon around 500 nm as it is observed in the experimental work. The SIF are coated with a single Langmuir-Blodgett monolayer for SERS/SERRS spectroscopy.

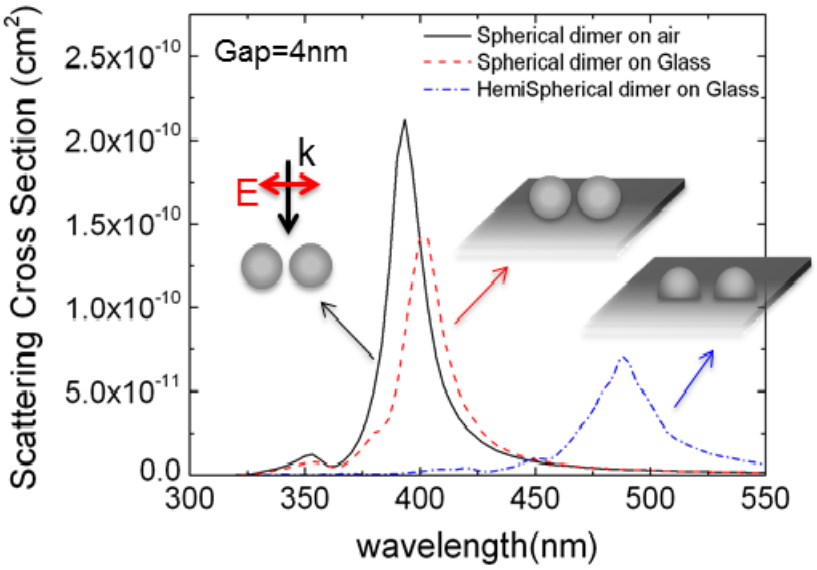

Figure 2.2 The properties of the coupling and the effect on the plasmon resonances

(Moula, G., et al., *Plasmonics and single-molecule detection in evaporated silver-island films.* Annalen Der Physik, 2012. 524(11): p. 697-704)

The properties of SERS spectra, can be discussed using a working definition of plasmon enhanced Raman scattering by Moskovits[4]:

> *"As it is currently understood SERS is primarily a phenomenon associated with the enhancement of the electromagnetic field surrounding small metal (or other) objects optically excited near an intense and sharp (high Q), dipolar resonance such as a surface-plasmon polariton. The enhanced re-radiated dipolar fields excite the adsorbate, and, if the resulting molecular radiation remains at or near resonance with the enhancing object, the scattered radiation will again be enhanced (hence the most intense SERS is really frequency-shifted elastic scattering by the metal). Under appropriate circumstances the field enhancement will scale as E^4, where E is the local optical field."*

This definition can be used to help the planning of experiments and interpretation of results.

The phenomenon of surface enhanced fluorescence requires an especial discussion due to the competing effects of the enhancement with the energy transfer or quenching. A complete classical treatment of the energy transfer of exited molecules on metal surface can be found in the review by Chance et al.[30] The subject have been revisited and discussed very recently in the literature.[31, 32] The authors of the latter work develop a model that confirms the quenching effect is observed in fluorescence but not in normal Raman. As it was already known, the quenching establishes limits for attainable enhancement, of the two processes. For a discussion of quenching in fluorescence see the book by Lakowicz[24].

Therefore, when a chromophore is too close to metallic nanoparticles that supports Localized Surface Plasmon Resonance LSPR strong quenched will appear[33]. As a result of the direct energy transfer to the metal, a new non-radiative decay channel is created Γ_{nR}^{Int}.

$$Q = \frac{\Gamma_{rad}}{\Gamma_{rad}+\Gamma_{nR}^{metal}+\Gamma_{nR}^{Int}} \qquad [2.6]$$

Where, Γ_{rad} is the radiative decay rate and Γ_{nR}^{metal} is the non-radiative decay rate. SEF and quenching are the two opposed outcome, which can be controlled by the separation and the distance between the metal and molecule. (18-19) A transition from quenching to enhancement should be noticed with the increasing of the distance between the molecule and the metal (14,20,21). Experimentally, using shell-isolated nanoparticles (SHINs) with different distance separations, SEF can be clearly demonstrated, and this technique has

been named SHINEF. SHINs particles can be delivered to target by different methods. The enhancement factor is multivariate function, including the shape and size of nanoparticles of mainly silver or gold. Also the dielectric constant of the surrounding medium can be a factor.

SHINs were synthesized by following method described by Li et al. (23) Gold core in the first stage was synthesized by reducing gold in tetrachloroauric acid ($HAuCl_4$). A 50 ml of 0.01% $HAuCl_4$ solution was brought to a boil over a hot sand bath then a solution of reducing agent (1 % sodium citrate) was added. The boiling was continued for 15 minutes and then was removed from heat and keeps stirring for another 15 minutes.at this stage the Au core was coated with silane coupling agent (3 mL of a 1 mM of 3-aminopropyltrimethoxysilane (APTMS), at vigorous stirring). The solution was heated in sand bath until reached 90-95°C then the coating with SiO_2 shell which comes from activated 0.54 % sodium silicate solution (9 mL). The solution then was allowed to stand for 3 hours with keeping the temperature at 90-95°C. Figure 2.3 provides sketch of the surface reactions involved in the formation of the thin silica shell on citrate.

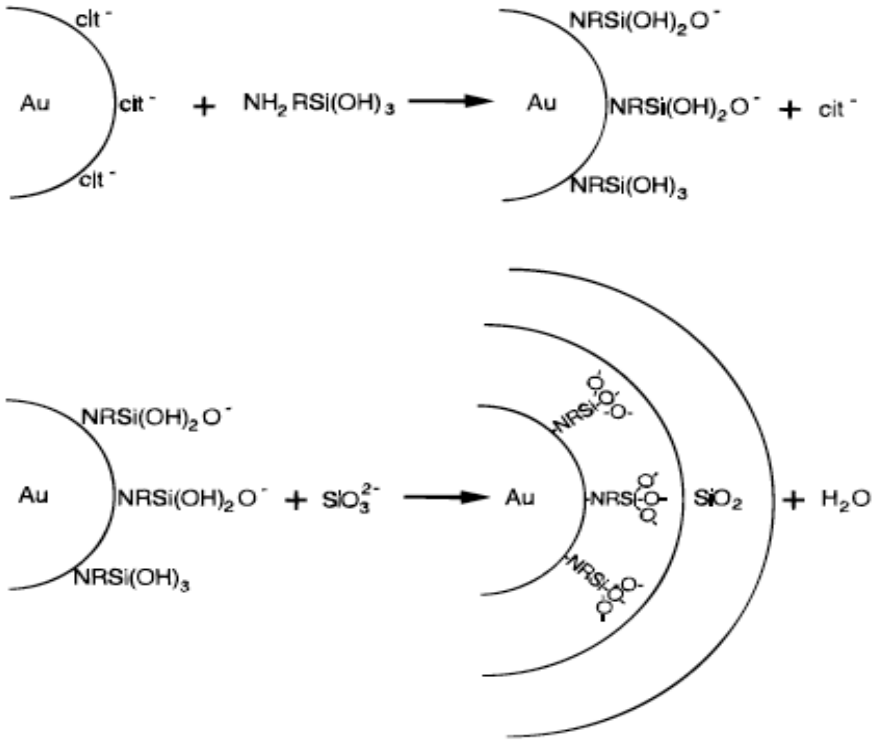

Figure 2.3 Sketch of the surface reactions involved in the formation of the thin silica shell on citrate stabilized gold particles (Liz-Marzan et al. Langmuir, Vol. 12, No. 18, 1996)

The silica shell has been chose as a shell around the gold core for many reasons. It can produce the strength, the inertness and even the possibility for conjugation with other materials, it can be delivered easily as smart dust, and make it stable by protecting the gold core. The SHINs solution can be delivered by drop coating on the tag-phospholipid monolayer fabricated on quartz slide and then let it to dry. In this thesis, we also explored the fabrication of SHIN films, with particles over silanized glass slide. The two delivering methods are used for Shell Isolated Nanoparticles Enhanced Fluorescence.

Chapter 3

Instrumentation Reviews

3.1 Langmuir Blodgett System

Thin organic films with thickness of a few nanometres are used in a wide range of scientific and commercial applications. These films of single or multilayers find their use in applications like sensors, displays, detectors and electronic circuit components. Various techniques have evolved which enables the synthesis of organic molecules of any required functionality combined with the more sophisticated technology of thin film technology. Some of the techniques used to deposit an organic thin film on a solid substrate are: thermal evaporation, sputtering, electrodeposition, molecular beam epitaxy, adsorption from solution, Langmuir-Blodgett (LB) technique[34, 35], self assembly, Layer-by-Layer (LbL). The films, allows the production of electrically, optically and biologically active components on a nanometre scale[36].

Among the various techniques used to deposit an ultrathin organic film on a solid substrate, the Langmuir-Blodgett technique is the most favourable since it allows (i) control over the monolayer thickness, (ii) uniform monolayer deposition over large areas and (iii) production of multilayer structures that can have altering layer composition. Another advantage of Langmuir-Blodgett technique is that it allows deposition of monolayers on almost all types of solid substrates[35].

3.1.1 History of Langmuir Blodgett System

In the year 1774, American statesman, Benjamin Franklin, dropped about a teaspoonful of oil in the water of a local pond and watched the droplet spread out rapidly and extend itself and it the process make the area within look crystal clear.

More than hundred years later Lord Rayleigh speculated that an oil film on water spreads and extends until the thickness of its layer becomes that of a molecule. At around the same time a German scientist; Agnes Pockles, established the surface contamination as function of area of the surface for the different types of oil, by using her own kitchen sink as fundamental surface balance. This work of Pockles was published in the year 1891 and served as the very basis of the quantitative work of Langmuir on alcohol, fatty acids and ester monolayers in the late 1910's and early 1920's. Irwing Langmuir was the first person to conduct systematic studies on monolayers floating on water and went on to win the Nobel Prize for his work. In the early 1920's Langmuir also reported the transfer of monolayers of fatty acid from the surfaces of water on to the solid substrates. But a more elaborate definition of such monolayer transfer (sequential monolayer transfer) was given later by Katherine Blodgett. Hence these built-up monolayer assemblies are called Langmuir-Blodgett (LB) films and the floating monolayers are referred to as Langmuir films.

It was still years later that scientific communities around the world realized the importance of the Langmuir-Blodgett technique. The year 1979 saw the first International Conference on the Langmuir-Blodgett technique being held. This was followed by the ever-increasing use of this technique by scientists and researchers working on different fields. Although the ultrathin organic films produced by the Langmuir-Blodgett (LB) technique has found feasible practical applications today, where LB films are used as model systems. A review of the LB work in surface enhanced spectroscopy has also been published.[37]

3.1.2 Definitions

a) Surface Tension

In a liquid, there exists a force of attraction between the molecules. This force of attraction is called cohesion and depends on the properties of the substance. When a liquid is present in bulk this interaction between the molecules is balanced as the each molecule in the bulk experiences equal force of attraction in all the directions. But for the molecules at the surface of the liquid these forces are not balanced as at the gas (air)-liquid (water) interface the force of attraction of the liquid is higher than that of the gas (air). Hence there will be a net force of attraction acting towards the liquid and under the action of this force the air-water will contract resulting in a reduction in its area.

This condition results in free energy that is present on the surface of the liquid and is known as the surface free energy. We can also define surface energy as the cohesive energy (resulting from the imbalance in the cohesive force) that exists on the surface of the liquid. Units for surface tension are dynes/cm or mN/m.

The molecular interactions for a polar liquid, like water, are stronger and hence such liquids have high surface tension. Decrease in the strength of the molecular interactions will automatically lower the surface tension. Some the factors that affect surface tension are:

(i) Temperature: Increase in temperature of a system will lower the surface tension.

(ii) Contamination: Contamination of any types, especially by surfactants, will bring about a reduction in surface tension.

(b) Surfactants

Surfactants are surface-active agents. These molecules usually consist of both hydrophilic and hydrophobic parts. The hydrophobic part usually contains hydrocarbon and fluorocarbon chains and the hydrophilic part contains the polar groups like –OH, -COOH, $-NH_3^+$, $-PO_4^-(CH_2)_2NH_3^+$.

In solutions the association behaviour of the surface-active agents (surfactants) results from their amphiphilic nature.

(c) Insoluble Monolayers

There are many surfactants that are amphiphiles and highly reduce the surface tension of water and form a monolayer at the interface. There are also many more molecular systems, insoluble in water, and with aid of a solvent, can be spread on the surface of water to form a monolayer at the air-water interface. Floating monolayers are called Langmuir films. The orientation of the molecules at the air-water or oil-water interface is controlled by the amphiphilic nature of the surfactants. It is always in a way that polar head group is pointed towards water and the hydrocarbon tail points away from water and towards air. Now, to form an insoluble monolayer the hydrocarbon chain of the substance should be long enough. If the water insoluble hydrocarbon chain falls short of the required length, micelles are formed on the surface of the water. Micelles are soluble in water and because of their presence the formation of monolayer is hampered. Furthermore formation of monolayer is also prevented if the water insoluble hydrocarbon chain is too long, as it tends to crystallize on the surface of the water. The thumb rule for the adequate length is that the chain should have more than 12 hydrocarbons or groups in the chain ($(CH_2)_n$, $n>12$). But as the ability of forming a film of the hydrocarbon chain is

highly dependent on the polar part of the amphiphile it is still not easy to predict the ideal length of the hydrocarbon chain. Also the amphiphile must be soluble in some volatile and water soluble organic solvent. The most commonly used organic solvents are: chloroform and hexane.

3.1.3 Langmuir film balance

The Langmuir film balance consists of a trough, generally made of Teflon, which holds the subphase and prevents its leakage over the edges. Water is circulated in channels that are placed underneath the trough and thermostats the trough. There are barriers, made of Delrin, over the trough surface that can be moved to change its surface area. Delrin is a hydrophilic material, which is heavy and hence can easily hinder any leakage of monolayer underneath the barrier.

3.1.4 Surface Pressure- Area Isotherm

The measurement of surface pressure as a function of the surface area of water that is available to each molecule provides us with the two-dimensional thermodynamic monolayer properties. The measured surface pressure π is the difference between the surface pressure of pure water and that of the water covered with the monolayer, in Newton/meter. This is considered as the most important indicator of the monolayer properties. These measurements are performed at a constant temperature. This is known as a surface pressure-area isotherm which is rich in information on the stability of the monolayer[35].

3.2 Metal Deposition Vacuum System

Metal deposition vacuum system is widely used to fabricate SERS substrates. As the name suggests, it is used to create an metal island film by vacuum deposition.[38] The system consists of a tungsten boat that has a grip on the metal. Vacuum deposition is carried out by allowing high current pass through the tungsten boat. The passing of high current results is thermal evaporation of the Ag or Au metal. The entire process is performed at about 10^{-6} Torr.

The process, which is undergone for the generation of the metal film, can be divided into several physical stages. These are:

- Thermal evaporation, which is responsible for the change of the solid metal into the gaseous phase.
- The substrate plate, which is kept in the vacuum chamber, at a set temperature, allows the formation of metal clusters on the surface.
- If the conditions necessary for surface diffusion are maintained, which is usually the temperature of the substrate; nanoparticles are formed on the surface of the substrate.

Metal deposition vacuum system can be applied to any solid substrate when films of a particular mass thickness and high purity are desired.

The metal film morphology determines the degree of surface enhancement caused in surface-enhanced Raman scattering (SERS). The thickness and rate of deposition, roughness of the substrate, its temperature during deposition and annealing for initiation

of the growth of the grain after deposition are the factors which have a direct control on the structure of the film.

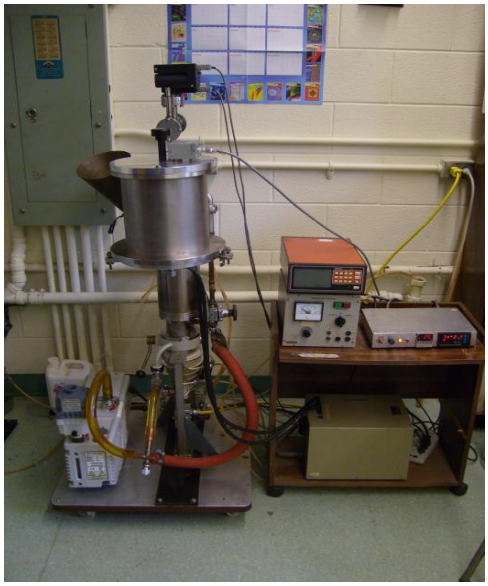

Figure 3.1 The Total System for Metal Evaporation (taken by author)

3.3 Synthetics procedure for Gold and Silver Shell Isolated

Surface-enhanced Raman spectroscopy is as a very powerful analytical technique. It is capable of generating non-destructive and extremely sensitive characterization down to single molecular level. In order to achieve the proper SERS effect substrates based on metals like Ag, Au and Cu are needed. These metals will have to be in the form of nanoparticles or roughened surfaces.

Recently, shell-isolated nanoparticle-enhanced Raman scattering approach was developed, where the Raman scattered signals are amplified using of gold nanoparticles with an ultrathin silica or alumina shell.[39]. The surface to be probed is covered with a monolayer of the nanoparticles called ‘smart dust’. The ultrathin coating:

- Prevents the nanoparticles from aggregating and becoming a lump,
- Prevents direct contact between the nanoparticles and the probed material, and
- Permits the nanoparticles to probe any surface.

In the approach of shell-isolated nanoparticle-enhanced Raman spectroscopy an Au coated nanoparticle is used instead of an Au tip. Each nanoparticle is covered with an ultrathin layer of silica or alumina and is similar to the situation of Au tips used in the TERS experiment[14]. The technique can be described as combining hundreds of Au tips together to form the nanoparticles, which are brought to the substrate surface to be probed. Also as the chemically inert shell coating prevents the nanoparticles from coming in direct contact with the substance to be probed, the shell-isolated mode is thus generated. The advantages of such isolation are the increased versatility and the wide range of practical applications. This technique is, thus, called the shell-isolated nanoparticle-enhanced Raman scattering (SHINERS).[39]

SHINs were synthesized by following method described by Li et al. (23) as discussed in chapter 2.

3.4 Surface and morphology characterization instruments

3.4.1 Scanning Electron Microscopy (SEM)

In scanning electron microscopy, different types of signals are produced at the solid surface by using a highly concentrated beam of high-energy electrons. The signals thus produced carry information about the specimen under scrutiny. Scanning electron

microscopy helps us determine the external morphology (texture), chemical composition, crystalline structure and the orientation of the materials that make up the specimen.

Fundamental Principle: The electrons that form the concentrated beam in scanning electron microscopy are accelerated, i.e., they posses large amount of kinetic energy. On coming in contact with the solid sample these electrons decelerate and there occurs a transfer of energy from the electrons to those emanating from the surface of the solid. Thus the signals produced are comprised of secondary electrons, backscattered electrons, diffracted backscattered electrons, photons, visible light and heat.

SEM is a non-destructive, which basically means that the X-rays generated by the electrons do not cause a loss in the volume of the sample. Hence the same sample can be used more than once for the analysis. The infrastructures required are: Power supply, Vacuum system, Cooling system, and Vibration free floor and at room temperature, which is free of any magnetic or electric field in the environment.

SEM is widely used in the development of high-resolution images of the shapes of different objects. It is also useful in the determination of spatial change in the chemical composition of the sample. It can also provide very accurate measurement of small object, in the range of 50nm as shown in Figure 3.2.

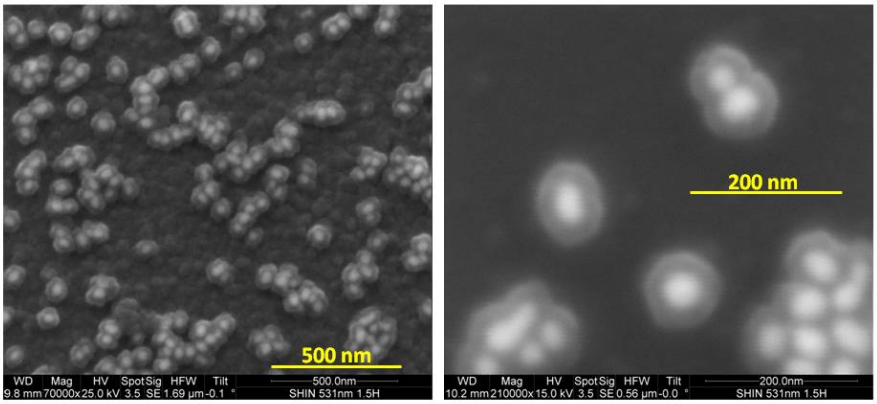

Figure 3.2 The accuracy in SEM images

Advantages

- SEM is arguably the only instrument, which has such wide range of applications in the examination and study of solids.
- SEMs are generally have user-friendly 'intuitive' interface and can be operated easily.
- In most of the applications there is minimal preparation required for the sample.
- Also in many applications the acquiring of data is simple and hence can be done rapidly.

Disadvantages

- SEMs have a microscopic chamber where in the sample are placed. So it is mandatory that the samples fit into this microscopic chamber. Maximum horizontal dimension is 10cm and the vertical dimensions should not exceed 40mm.

- Samples that are prone to decrepitation or likely to outgas at low pressure are not suited for the typical SEM.
- The EDS detectors with which the SEMs are equipped fail when very light elements are involved.

3.4.2 ATOMIC FORCE MICROSCOPY (AFM)

Scanning probe microscopes (SPMs) are used to measure morphology of surfaces[40]. These instruments are capable of carrying out the measurements with nanometric accuracy. The scanning probe microscopes involve both scanning tunnelling microscope and atomic force microscope.

The principle of the atomic force microscope technique is that when a tip, connected to a cantilever end, is brought within the inter-atomic separations of a surface, it leads to the development of inter-atomic potential between the atoms of the tip and the surface. This inter-atomic potential will cause the tip to move up and down complying with the surface profile as it travels across the surface. Thus, in order to be able to determine the topographical characteristics of the surface it is only required to measure the deflection of the cantilever. A laser and detector monitor the movement of the cantilever and also help in measurements of the forces between the sample and the tip. Also in order to limit the force of interaction to a preselected level, called the Reference Force, the sample is moved up and down with the negative feedback loop via a piezoelectric scanning tube. By recording the movement of the cantilever in the direction of the Z-axis expressed as a function of X and Y, a three dimensional image can be composed.

There are a variety of AFM imaging modes that are available. But the most common of them all are the contact and the non-contact (tapping) mode.

Contact Mode AFM: In this mode a sharp tip is connected to the end of a micro-fabricated cantilever. The tip along with a split photodiode detector scrutinizes and inspects the deflection in the cantilever while being in continual contact with the sample surface. The tip is regularly adjusted so that it keeps on maintaining the same deflection (or the same height above the sample surface). This helps in creating images, which displays the changes in height, friction and deflection. A feedback loop is used to maintain the constant deflection. This is done by vertical motion of the scanner at each of the data point so as to keep a set point deflection. Contact mode AFM cannot be used for soft sample as the tip, when moved while in contact with the surface, can cause harm to the surface by scratching it.

Tapping Mode AFM: In the tapping mode, the cantilever is oscillated close to the resonance frequency by the use of piezoelectric actuators. As a result, the tip, connected to the cantilever, touches the sample surface only at intervals. Thus, the tapping mode AFM can scan the sample surface without scratching it. Even in the tapping mode a feedback loop is used to maintain the amplitude of oscillation of the cantilever. Hence, as the tip moves over a rise on the surface of the sample the amplitude decreases due of space for movement of the cantilever. Similarly as the tip moves over a depression on the surface there is an increase in the amplitude since the cantilever gets enough space for movement. Thus, on the basis of the tip and the surface interaction there occurs a continual change in the amplitude, frequency and phase of the oscillation shift. Tapping mode AFM has proved to be ideal in the study of soft, easily damaged, nanoscale

structures due to its ability to bring about a noticeable reduction in the lateral forces couple with scanning. Figure 3.3 shows Tapping mode AFM image of Typical Silver Island Film

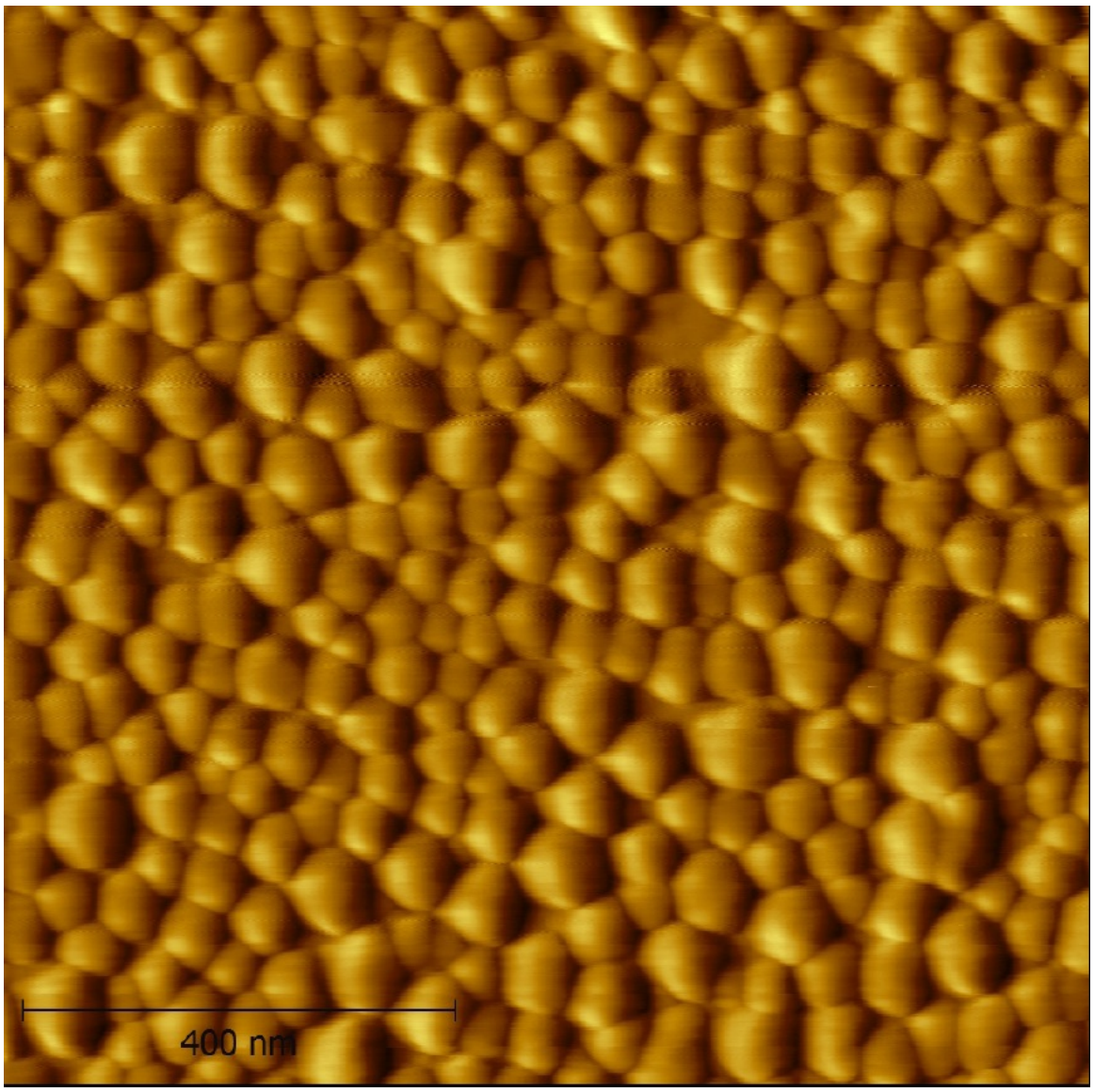

Figure 3.3 Tapping mode AFM image of Typical Silver Island Film

3.5 Spectroscopic characterization instruments

3.5.1 UV-Visible spectroscopy

The ultraviolet and visible spectroscopy is a technique, which has become an integral part of the modern day laboratory. This technique is probes the electronic absorption using ultraviolet and visible light for the analysis of materials, including complex metal ion in solution and organic compounds.

Ultraviolet and visible have ample amount of energy to be able to excite the electrons that occupy the levels of higher energy in a complex ion. So when visible radiation passes through a sample with full extent of its wavelength it produces an absorption spectrum. There is a characteristic absorption corresponding to each electronic transition. Substances appear coloured because they absorb the wavelengths of light in the visible region of the electromagnetic spectrum.

Radiation in the ultraviolet and visible spectrum can be used for generation of electronic transition in organic molecules. The only requirement in this case is a broadband light source with wavelength between 200-800 nm. This method is used as the first step in spectroscopic characterization of molecules and nanoparticles.

Ultraviolet and visible spectroscopy is useful in analysis and the identification of various substances and groups with multiple applications.

- In order to figure out the amount of trace metal in an alloy the metal sample is first reacted to make it into a solution as ion. The ion is then made further complex to get into a form, which can be easily measured. The spectrum of the complex ion is then recorded using which the absorbance (absorption coefficient)

is found. From the absorption coefficient the concentration of solution and hence mass of the metal in the sample can be calculated.

- Almost the same process is applied to drug metabolites.
- Ultraviolet and visible spectroscopy is used in optical fibres, which are added to toothpastes and detergent powders.
- For watermarks to show up under an ultraviolet lamp, ultraviolet absorbing inks are added to the watermarks.

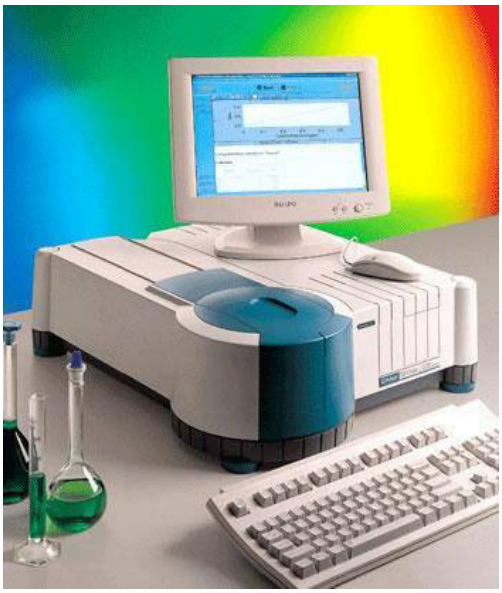

Figure 3.4 Cary UV-Vis Spectrometer (Adapted from EVISA)

3.5.2 Raman and Fluorescence spectroscopy

- **Raman Spectroscopy**

Raman Effect, as the name suggests, was discovered by an Indian physicist named Chandra shekhar Venkata Raman[3]. Raman Effect is basically the phenomena of inelastic scattering of light. The Raman effect describes the shift in wavelength for a

small fraction of radiation, which has been inelastically scattered by molecules, whose frequency differs from that of the incident beam. This shift in wavelength is dependent on the chemical composition and structure of the molecules that cause the scattering of the radiation. The scattered radiation is used in Raman spectroscopy to understand molecular vibrations, which, in turn, help throw light on the structure, symmetry, electronic environment and bonding of the molecule. And thus the quantitative and qualitative analyses of the individual compounds become possible[6].

There are two types of scattering, which results from the irradiation of a molecule with monochromatic light: elastic and inelastic. In the case of elastic scattering, there is no shift in wavelength and also change in photon frequency does not occur. In inelastic scattering there is a shift in wavelength and change in photon frequency. This happens because of the excitation or deactivation of molecular vibration in the process of which the photon may lose or gain energy[3].

Raman Spectrometer: Raman spectrometer consists of a source of light, monochromator, sample holder and a detector. There are two different techniques that are used to collect the Raman spectra. They are:

- Dispersive Raman spectroscopy, and
- Fourier transforms Raman spectroscopy.

They differ from each other in their laser sources and also in the way in which Raman scattering in detected and analysed. The methods have their own unique advantages and disadvantages and hence the choice of the type of method is solely dependent on the sample. Effective FT Raman spectrometers were developed using red excitation lasers.

This helped overcome the issue of preventing fluorescence that affects the Raman signals in strongly absorbing molecules. Moreover, the capacity of analysis was highly improved with the invention of extremely sensitive detectors combined with coupling of optical fibres and microscopes.

There are different types of lasers that can be used for the purpose of excitation, such as: argon ion (488.0 and 514.5 nm), krypton ion (530.9 and 647.1 nm), He: Ne (632.8 nm), Nd: YAG (1064 nm and 532 nm) and diode laser (630 and 780 nm). Fundamentally, during vibration if there is a change in polarizability of a molecule, it is said to be Raman active.

Raman spectroscopy is also used in combination with a lot of hyphenated analytical techniques. Some of these techniques are: high-performance liquid chromatography, micro chromatography, scanning tunnelling microscopy, atomic force microscopy.

Advanced Raman Techniques

(i) Surface Enhanced Raman Spectroscopy (SERS): SERS is a great improvement to the Raman scattering signal. It is a tool used for the detecting adsorbate molecules on rough metal surfaces. This technique was discovered by R. Van Duyne[11].

(ii) Resonance Raman spectroscopy (RRS): For resonance Raman spectroscopy the energy of photon of an exciting laser and the energy required for electronic transition should match each other. Enhancement in Raman bands is particularly high for specific molecular vibration. The most common is the Frank-Condon enhancement. In this category the normal coordinate of vibration has one of its component in the molecule's direction, which expands during electronic excitation.

- **Fluorescence Spectroscopy**

All fluorescence measurements in our work are carried out using the Invia micro-Raman system.

Fluorescence occurs when a molecule absorbs light of the proper wavelength, it is excited to one of the excited electronic states.[24] These excited electronic states have many vibrational levels. Once the molecule has moved from the ground state to the excited electronic state, relaxation occurs, as explained in chapter 1.

Fluorescence and its various applications have highly improved in the past decade. Development in time resolution, data analysis methods and better instrumentation in the past decade has led to a rise in the level of interest in fluorescence. In addition to these the recent development in laser and detector technology also has an important part to play in creating added interest in fluorescence.

Fluorescence spectroscopy has proven to be a promising technique in the field of diagnosis as it has the ability to carry out quick and rapid diagnosis. In the field of medical microbiology fluorescence spectroscopy has been termed as the ultimate diagnostic tool. Studies are being carried which suggest that fluorescence spectroscopy may prove to be an impeccable technique in the detection of viruses.

Chapter 4

Self-assembly of shell isolated silver nanoparticles on silanized glass surfaces

The objective of this chapter was the preparation of enhancing substrates through self-assembling of shell isolated nanoparticles of Ag on silanized glass. The coupling agent or linker used is 3-amino propyl triethoxysilane. The surface density of nanoparticles increases with the immersion time of the silanized glass in the SHINs solution. Their self-assembly on glass that had been silanized is determined for several deposition time intervals: from three to sixteen hours. The surface coverage was monitored by AFM imaging.

The role of localized surface plasmon resonances in isolated metallic nanoparticles provide simple models for the observed SERS and SEF and for the design of practical applications.[5, 17] However, it has become evident that plasmon coupling plays fundamental role, particularly at spatial locations known as hot spots[41]. The basic idea is to fabricate reproducible enhancing substrates with controlled performances that might give rise to high factors of amplification. Xu et al[42] presents calculations that show that 10^{10} electromagnetic improvements exist between any nanospheres that have a space of up to 1 nm between them. In practice, findings forecast that in applications of SERS, aggregates form more efficient enhancing substrates compared to separate nanoparticles. Large enhancements are detected at "hot spots" in aggregates of nanoparticles.

Molecular emission is represented by the following equation:

$$I_0 = I_{exc} \times \varepsilon \times Q_0 \qquad [4.1]$$

Where I_0 is the fluorescence intensity, I_{exc} is the excitation intensity, ε is the absorption extinction coefficient, and Q_0 is the intrinsic quantum yield. While the quantum yield is expressed in terms of lifetime or decay rates as follows:

$$Q_0 = \frac{\Gamma_{rad}}{\Gamma_{rad}+\Gamma_{nR}} \qquad [4.2]$$

Where Γ_{rad} is the radiative decay rate, and Γ_{nR} is the non-radiative decay rate.

Several changes will occur when the chromophore near metallic nanoparticles that support LSPR. The absorption profile will intensify due to the new local electric field near the nanoparticles when its surface plasmon is excited, and then the fluorescence will modify.

Coupling between two local electric fields occurs in neighboring nanoparticles (hot spots). This produces large enhancement values due to the highly localized area between the nanoparticles.

Wide-range of nanostructures that are confined to surfaces and that facilitate the regulation of plasmonic characteristics as well as the enhancement of optical signals may be generated by many fabrication strategies which include electron beam and nanospheres lithographies.[43] The latter applies to both enhancement off light scattering and emission.[44] In this work we present the immobilization of Ag SHINs through nanoparticles' self-assemblage. An attempt is made to fabricate substrates for SHINERS[39] and SHINEF[45] through the self-assembling of metal-coated nanoparticles, a bottom-up method. The constituent blocks in this regard are shell isolated silver nanoparticles. The immobilization of NPs in a glass slide can be achieved with the help of linkers. The overall selections of linkers of self-assembly that are non-covalent are often polymers as well as polymeric dendrimers along with proteins. For the self-assembling involving covalent linkers the characteristic selections are dithiols and organic

type of silane. Bottom up methods, unfortunately, are limited and cannot offer spatial reproducibility when compared with nanolithographic approaches.

In this chapter, shell isolated nanoparticles of silver citrate are utilized for self-assembly. The coupling agent or linker used is 3-amino propyl triethoxysilane. It is used for coupling the NPs to microscopic slides of glass. Glass surfaces are silanized and Ag-SHIN nanoparticles are adsorbed onto the surface.

Electrostatic forms of interactions using the dipping strategy facilitate both the silanization as well as deposition. Controlling the deposition time regulate the degree of the aggregation of the nanoparticles. Particles come quite close to one another with increased of surface particle concentration through long deposition times. Increasing nanoparticles concentration per unit area brings about more junctions between particles.

4.1 Experimental

Silver nitrate, nitric acid, sulfuric acid, trisodium citrate, hydrochloric acid, 3-amino propyl triethoxysilane, anhydrous acetone, chloroform as well as sodium silicate were purchased from Aldrich. There was no additional purification of any of them prior to their use. Ag SHINs at about 55 nm were synthesized according to the standard sodium citrate reduction method. In a round bottom flask equipped with condenser, a 36 mg of $AgNO_3$ into 200 mL milli-Q water was brought to boil with vigorous magnetic stirring. In typical procedure, 4 mL of 1% sodium citrate **($Na_3C_6H_5O_7$)** was added. The solution left for 1 hour at high temperature and vigorous stirring. As initial step of coating, 12 mL of a freshly prepared 1mM APTEMS (3-aminopropyltriethoxysilane) to the resulting solution under vigorous stirring for 15 min. The coating then was performed by adding 36 mL of activated 0.54% aqueous sodium silicate solution (pH 10.5). The solution then was allowed to stand for 3 hours in sand bath (220^0C) and vigorous stirring. All the glass apparatus that were utilized were cleaned using aqua regia. Notably, aqua regia is a mixture of HCl together with HNO_3 in a 3:1 ratio. The water that was utilized in the entire experiment was doubly distilled and adding a system of Milli Q from a Millipore for its purification. The resistivity of the water at 25^0C was in excess of 18.2 MΩ cm. For silanization, the surface of Corning 2048 glass slides, measuring 25 cm by 75 cm, were cleaned in a solution containing 50v/v sulfuric acid for about three hours. Thereafter, they were severally rinsed using Milli-Q water through sonication, then, they were placed in ambient temperature settings, free from dust, to dry. The slides that had been cleaned were immersed, for eight minutes, in a 2% 3-amino propyl triethoxysilane solution in acetone. Following the silanization, the slides were cleaned using Milli-Q water so as to

get rid of the extra silanes on the surface. After the silanizationof the slides they were put into a solution of SHIN nanoparticles to commence deposition through self-assembling. The latter is possible via linkages of amine molecules that bore positive charges from the surface of the slides and Ag SHINs that bore negative charges. The SHINs particles that were not bound were eliminated using Milli-Q water.

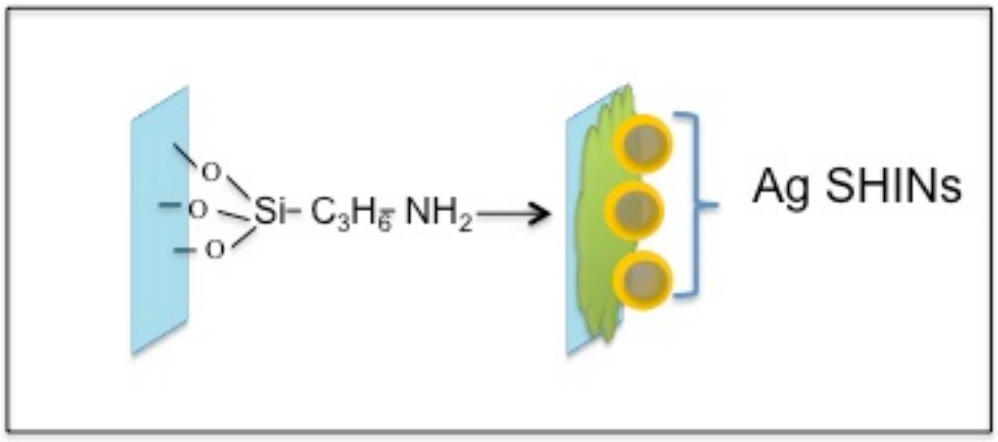

Figure 4.1 A schematic cartoon showing the deposition of the particles

A schematic cartoon showing the deposition of the particles is presented in Figure 4.1. The time spent immersing the substrates that had been silanized in a solution of Ag SHINs allows for the regulation of the density of the nanoparticles per unit area. Through trial-and-error, several immersion times were tested. In this chapter, the results are presented for the slides that had been silanized, after six, twelve and sixteen hours of the deposition of SHINs.

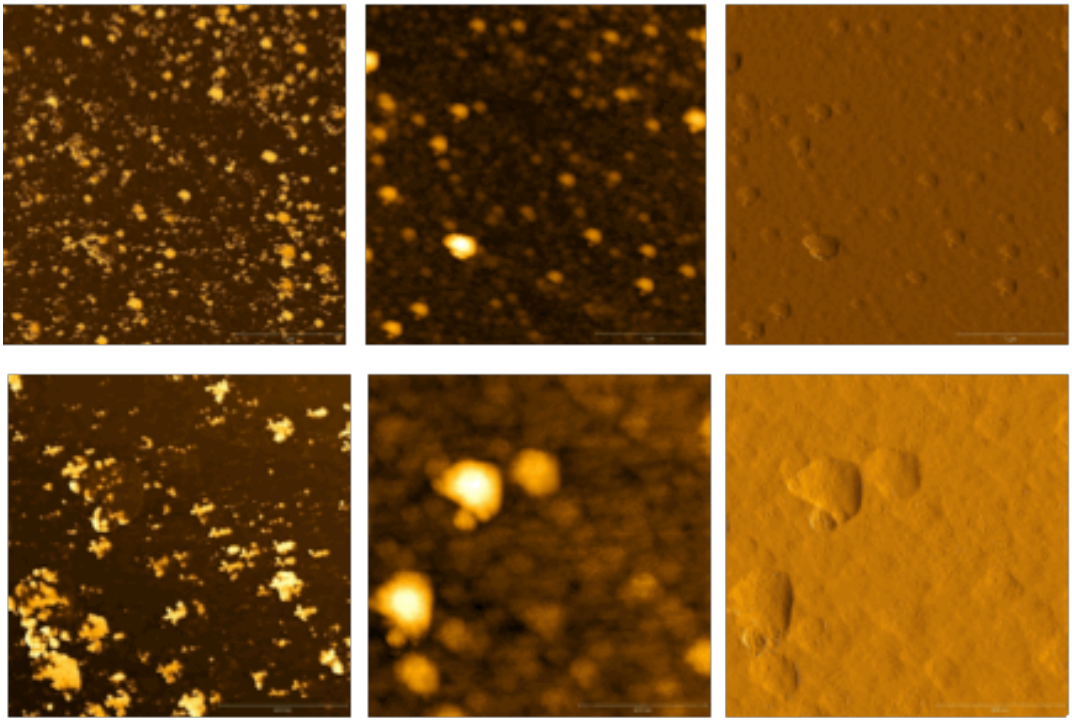

Figure 4.2 AFM images using tapping mode of silanized glass of 16 hours deposition time of Ag SHINs

Chloroform of pure grade was utilized to prepare solutions of Octadecyl Rhodamine B chloride R18, for the formation of Langmuir monolayer. Drop-wise, the solution was cautiously spread on the surface. This was done through dropping the solution through a microsyringe that was held quite close to it. We let the solvent to evaporate for close to half an hour. The subphase comprised of 18.2 MΩ cm of Milli-Q water, at a constant 25^0C temperature. This was followed by the compression of the monolayer at a constant barrier velocity of 6 cm^2min^{-1} to document the pressure at the surface.

The pressure is determined using a Wilhelmy sensor. The monolayer film was transferred using Z-deposition with a dipping device controlled electronically. The transfer was conducted at a constant pressure of 25 $mN.m^{-1}$, and the transfer ratio was near unity. LB

monolayers of Octadecyl Rhodamine B chloride R18 were therefore transferred onto films made of silver SHINs.

UV-Vis absorption type of spectra was used to monitor the Octadecyl Rhodamine B chloride R18's solution, the dispersions of silver silicate as well as the films made of silver with the help of a Cary 50 Scan UV-Vis type of spectrometer. The Ag-SHIN films had been generated through self-assembly on surfaces that had been silanized. The AFM (atomic-force microscopy) images were obtained using Digital Instruments Nanoscope IV, was operated in a non-contact tapping mode using an n^0 tip of silicon. The fluorescence spectra of the monolayers films made from LB were measured in the Renishaw Invia system equipped with a 514.5 nm laser excitation, applying 10 to 20 μW power on samples so as to avoid any possible photodegradation. Every measurement was in a backscattering geometry using a 50x objective on the microscope, which provided ca.1μm^2 of probed surface area.

4.2 Results and Discussions

Surface coverage and morphology was monitored using AFM images for 16 hours time deposition indicating the generation of Ag SHINs aggregations, as shown in Figure 4.2. Figure 4.3 shows the plasmon absorption spectra of silver SHINs in solution. The reference absorption spectrum of the $1.34x10^{-4}$ M Octadecyl Rhodamine B chloride R18 solution, and the reference fluorescence spectrum of R18 LB monolayer. The absorption of the plasmon indicates a broad spectrum that covers the range of the emission. The latter hints the existence of broad distribution of sizes of nanoparticles. The absorption spectra of the molecule with the broad maximum at 557 nm resonated well with the wavelength of laser excitation at 514 nm.

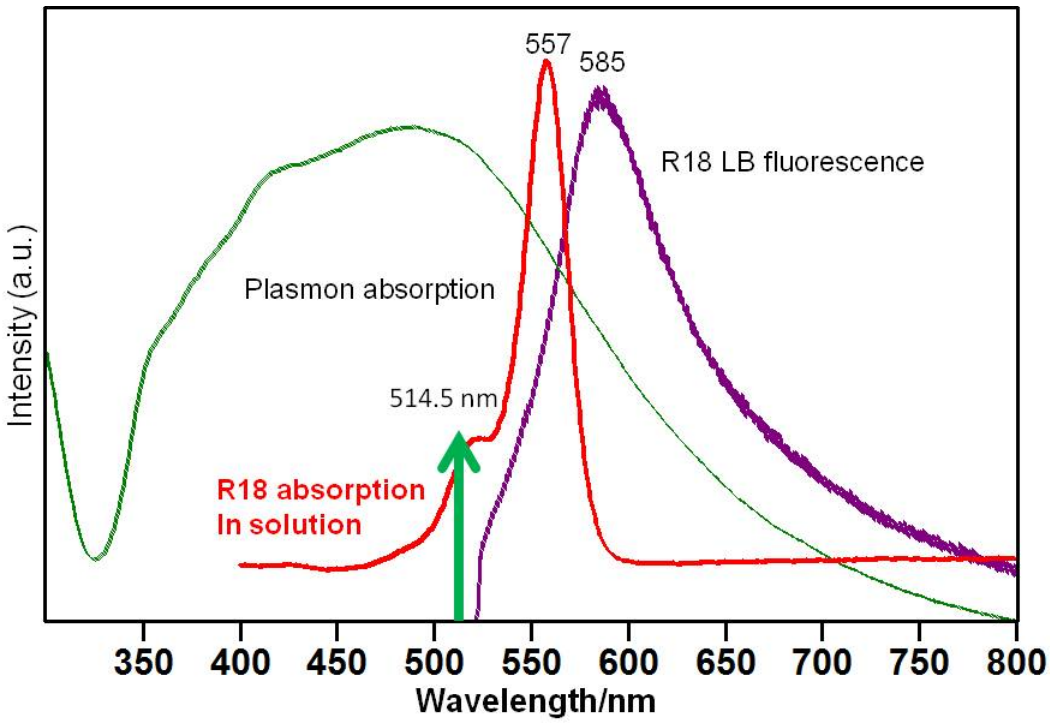

Figure 4.3 The plasmon absorption spectra of silver SHINs in solution, Octadecyl Rhodamine B chloride R18 solution and LB emission spectrum of R18

The Ag-SHINs films were produced through self-assembly on surfaces of glass that had been silanized using varied periods of immersion: six, twelve and sixteen hours (Figure 4.4). This provides an insight into the growth of nanoparticles on surfaces that are silanized. The nanoparticles' density goes up with increasing periods of deposition. Thus, the shape along with intensity of the absorption of plasmon is varying partly owing to supplementary coupling. The figure also show that the surface of glass were completely silanized, allowing for the increase in the attachment of Ag-SHIN particles with the immersion time.

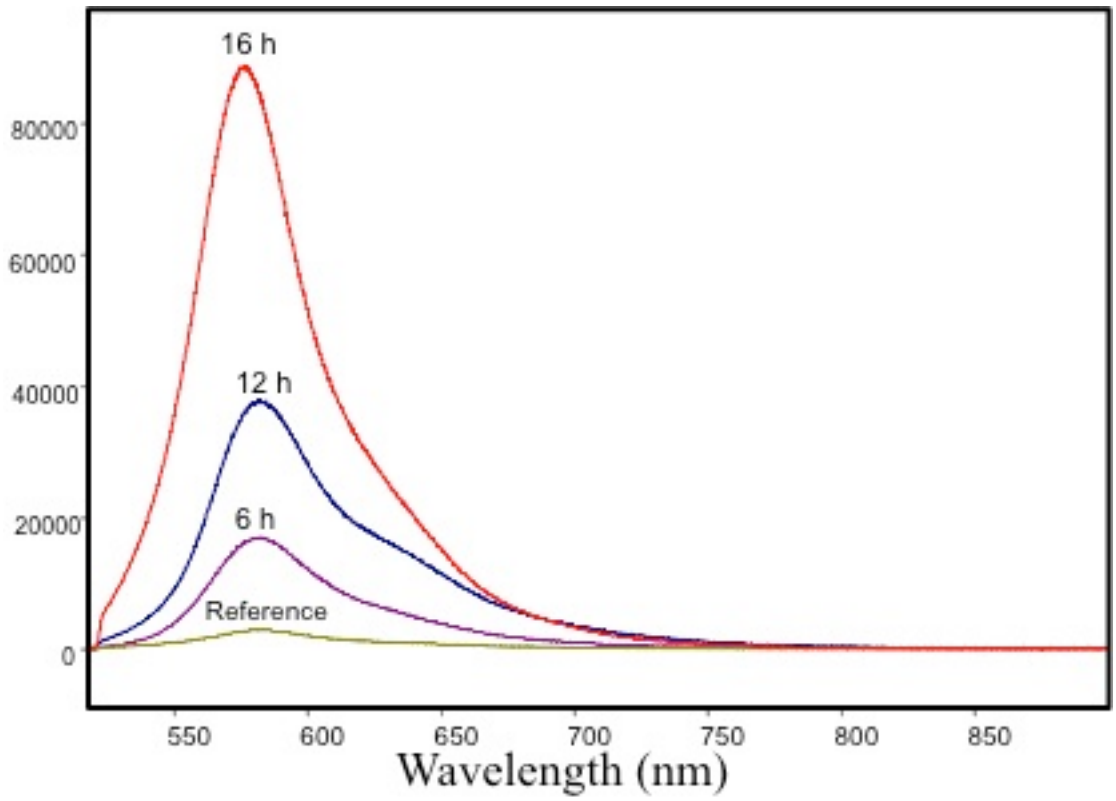

Figure 4.4 The Ag-SHINs films on surfaces of glass that had been silanized using varied periods of immersion: six, twelve and sixteen hours and reference

Fluorescence enhancement is observed for the target molecules of R18 in all cases and SHINEF is observed. Notably, in the literature, SEF is also referred to as MEF (metal-enhanced fluorescence)[46]. The Ag-SHINs are an experimental demonstration of the SEF distance the dependence shown by Wokaun[47] in mid 1983, and numerous other teams have confirmed similar trends. Additionally, within SEF the only field that is enhanced is the incident one providing an E^2 dependence, while enhancements of SERS attain amplification (E^4 dependence) from incident and scattered fields [48].

SHINEF spectra from the monolayer of R18 on the substrate made of Ag-SHINs after six and sixteen hours of immersion time are depicted in Figure 4.5. The R18's inherent quantum yield is ca. 0.7, and the attained mean factor of enhancement was forty.

The image obtained through AFM for a sixteen-hour long deposition depicted within the inset indicates the generation of aggregates

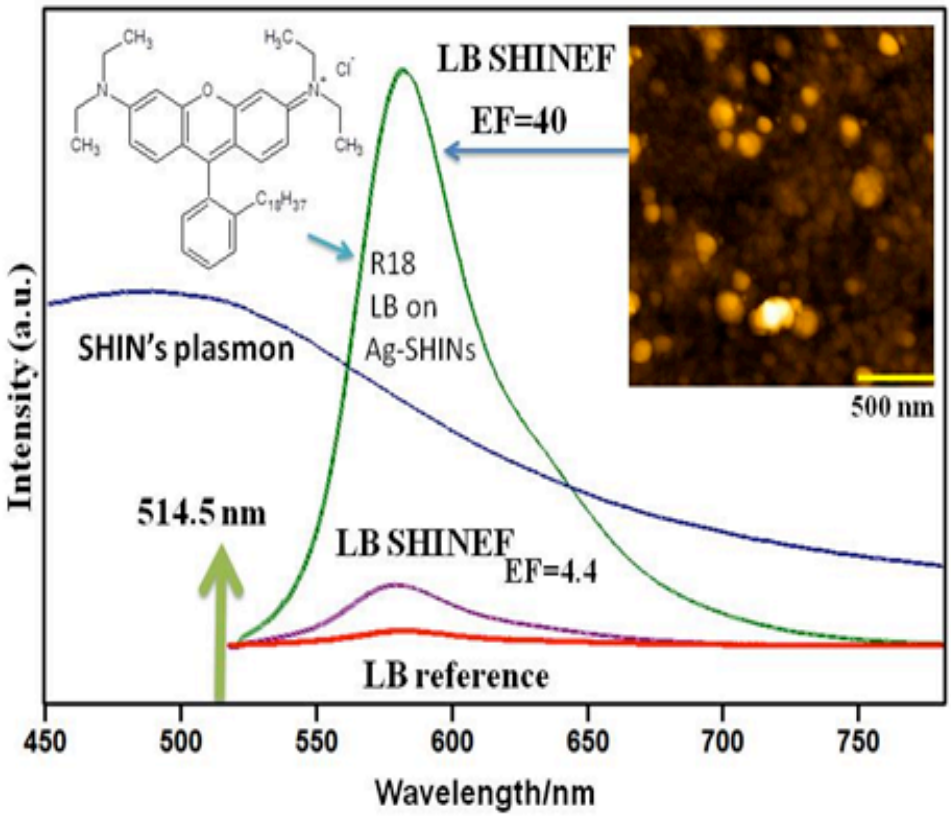

Figure 4.5 The monolayer of R18 on the Ag SHINs and spectra of SHINEF after six and sixteen hours

4.3 Conclusions

In this project, the preparation of enhancing substrates through self-assembling coated colloidal nanoparticles of Ag is presented. The approach is a *bottom up* method, where Ag-SHIN nanoparticles are the constituent blocks. The coupling agent or linker used was amino functional silane or 3-amino propyl triethoxysilane. The nanoparticle density goes up with increasing periods of deposition. Thus, the shape along with intensity of the

absorption of plasmon is varying partly owing to supplementary coupling. The outcomes shows that the best SHINEF enhancement (enhancement factor of ca.40) is attained on surfaces where the Ag-SHINs form aggregates, similarly to what is normally observed on SERS experiments on colloidal silver.

Chapter 5

Plasmon enhanced scattering and fluorescence of phospholipids in Langmuir-Blodgett monolayers

In this chapter we present the results of the investigation of *N*- (Fluorescein-5-Thiocarbamoyl)-1,2-Dihexadecanoyl-*sn*-Glycero-3-Phosphoethanolamine, Triethylammonium Salt (*fluorescein DHPE*) exposed to Au-SHINs to attain SHINEF, and vacuum evaporated silver island films employed as SERS/SERRS substrate for enhanced scattering.

While lipid bilayers underpin the structure of biological membranes universally, the lipid fractions of the biological membranes are fused with phosphate group, forming phospholipids bilayers. Langmuir-Blodgett (LB) films can be formed of mono- or bi-layers of organic material deposited on a solid surface, therefore useful for mimicking biological membranes. The artificial bilayer structures of lipids and phospholipids can be fabricated using the LB technique[34, 35]. LBs have been extensively used for the analytical and structural studies of single monolayers, bilayers and multilayers[49]. Ideal lipid membrane models have remained pivotal in the field of chemical biology and pharmacology, for effective molecular recognition trying to understand the architecture of biological assemblies and biological functions. Thus, physical and chemical interactions between immobilized biomolecules and drugs or biopharmaceuticals (proteins), can be studied using artificial lipid membranes such as LB. In such studies, diffusion, protein-folding membrane interactions, and DNA sequencing of the probed molecules can be examined by single-molecule spectroscopy, which allows tracking behavior of individual molecules, through the attached chromophores[50]. In terms of ultrasensitive detection and molecular characterization, the advantages of SERS/SERRS spectroscopy are obvious, since they provide molecular fingerprints and identification of functional groups observed as narrow lines in the inelastic scattering spectra.[4, 5]. Fluorescence

spectroscopy and SEF can be considered complementary, providing ultra sensitivity of probed molecules through broadband emissions[51, 52]. SERRS spectroscopy utilizes the vibrational Raman spectrum, which is rich in molecular behavior information in contrast to fluorescence. However, Raman spectral cross-sections of phospholipids are very small, therefore attaching chromophore is a necessary condition to approach single molecules detection using SERRS[53, 54]. Furthermore, SERRS confers two resonance enhancements, per se. The resonance Raman scattering effect can be achieved by fine-tuning the excitation frequency to match the electronic absorption band of the attached chromophore, with RRS cross-sections that can be up to 10^{-25} cm^2/molecule[55]. In addition, local field enhancements can be attained through excitation of surface plasmons in metal nanostructures with an approximate E^4 plasmon enhancement[56]. In the present wok, a dye-tagged phospholipid *fluorescein DHPE* (structure shown in Figure 5.1) is used for ultrasensitive detection experiments.

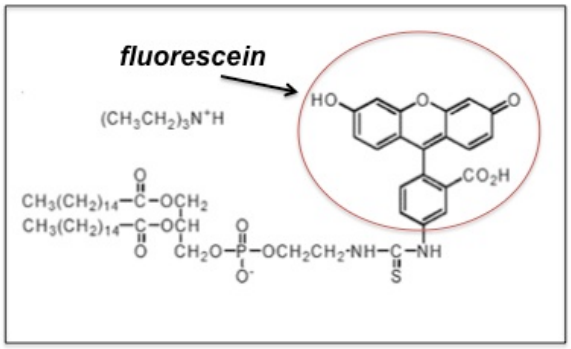

Figure 5.1 Illustration for chemical structures of the tagged phospholipid

5.1 Experimental details

N- (Fluorescein-5-Thiocarbamoyl)-1,2-Dihexadecanoyl-*sn*-Glycero-3-Phosphoethanolamine, Triethylammonium Salt (fluorescein DHPE) was obtained from Invitrogen and used as received. Arachidic acid (AA- the saturated fatty acid with a 20 carbon chain- $CH_3\left(CH_2\right)_{18}COOH$), chloroform, and ultrapure (99.9%) Ag shot (1-3 mm) were purchased from Aldrich, and used without further purification. All solutions were prepared using spectroscopic-grade chloroform as the solvent. Silver island films (SIF) of 6 nm mass thickness were vacuum evaporated onto Corning glass microscope slides at a pressure of 10^{-6} Torr while keeping a substrate temperature of 200^{o} C (that was maintained for 1 hour after evaporation). Langmuir monolayers containing mixed monolayers of *fluorescein DHPE* and Arachidic acid at different concentrations were prepared and added drop wise at the air-water interface of a Mina Langmuir trough to form a monolayer to be transferred onto silver island film (for SERS/SERRS) and quartz slides (for SHINEF).

The area per molecule in mixed AA: *fluorescein DHPE* LB films is about 25 Å^2, so for 1 μm^2 there is ca. 4×10^6 molecules required to cover that area. One target molecule in 4×10^6 molecules is required to reach one molecule of the chromophore per 1 μm^2. The concentration of *fluorescein DHPE* in the stock solutions was 10^{-4}M.

Langmuir monolayer is formed after adding 200 µL of the AA: *fluorescein DHPE* solution mixture onto a pure water subphase (18.2 MΩ.cm) at room temperature of 23^{o} C (surface pressure ca. 73.5 mN/M), after allowing the solvent to evaporate the film was ready to transfer. Nima Langmuir trough model 302M electronically controlled dipping

devices were used to transfer film. The compressing was at 6 mm/min until reached 25 mN/m. Transferring the monolayers onto immersed glass side covered by 6nm silver island film and quartz slides at a rate of 2 mm/min using Z deposition.

UV-visible absorption spectra were recorded with a Cary 50 scans UV-visible spectrophotometer for all solutions, Au SHINs solutions and 6 nm mass thickness silver island films. Atomic force microscopy (AFM) images were recorded through a Digital Instruments Nano-Scope IV operating in tapping mode with an n^+ silicon tip. The plasmon and molecular absorption spectra and the AFM image of a typical silver SIF are shown in Figure 5.2. Gold nanoparticles coated by SiO_2 were synthesized using the procedure reported by Li et al.[39] as discussed in chapter 2.

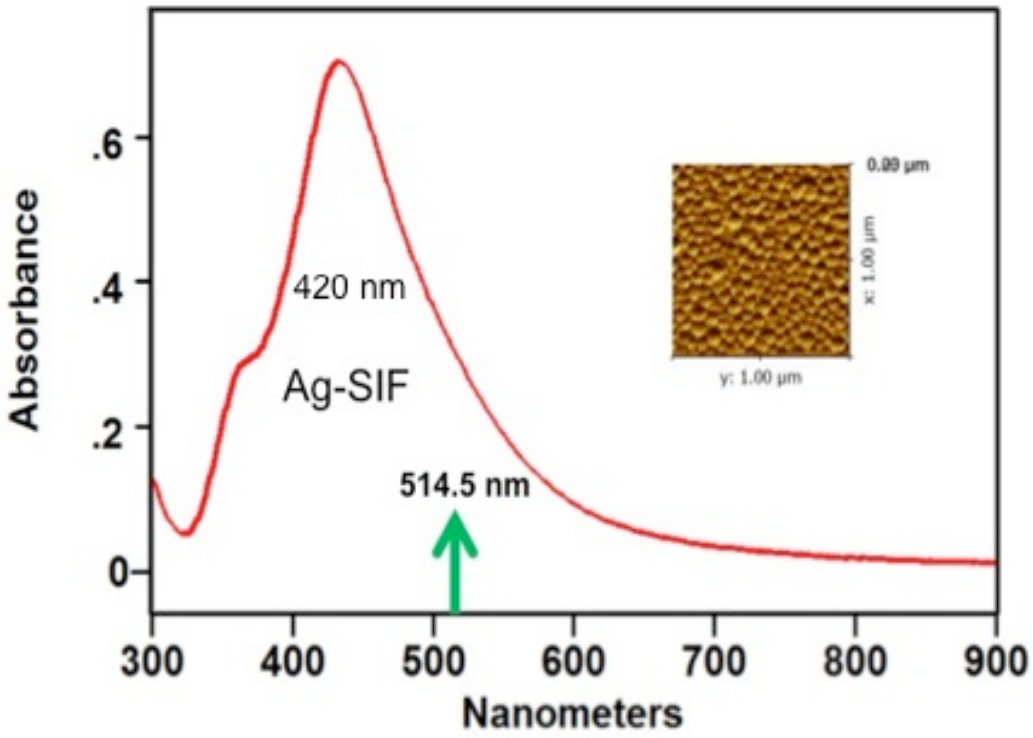

Figure 5.2 Extinction spectrum of a typical Ag-SIF on glass and AFM phase image of 1µm^2 surface area

Raman scattering and fluorescence were recorded in micro-Raman system in a backscattering geometry. The microscope is equipped with a 50x objective with a numerical value of the aperture of 0.75. The latter provides a field of view of ca.1μm^2 of surface area. The mixed LB monolayers on SIF films were probed using a 514.5 nm laser excitation and that applying 10 to 20 μW of power at the samples so as to avoid photodegradation. Spectra were recorded with a 4 cm^{-1} resolution, and 10 seconds accumulation, unless otherwise indicated.

5.2 Results and Discussions

5.2.1 Langmuir and LB films

The Langmuir technique was employed to obtain surface pressure area per molecule, (π-A) isotherm of *fluorescein DHPE* monolayers[34, 35]. A typical isotherm is shown in Figure 5.3. Gaseous phase is observed at molecular area larger than 150 $Å^2$, the monolayer then shifts to a liquid- condensed phase with additional compression, until the monolayers collapsed at pressure around 40mN/m. the isotherm exhibits typical liquid expanded behavior which is related to the reorientation of phospholipid chain. The monolayer was transferred to silver island films at pressure of 25 mN/m.

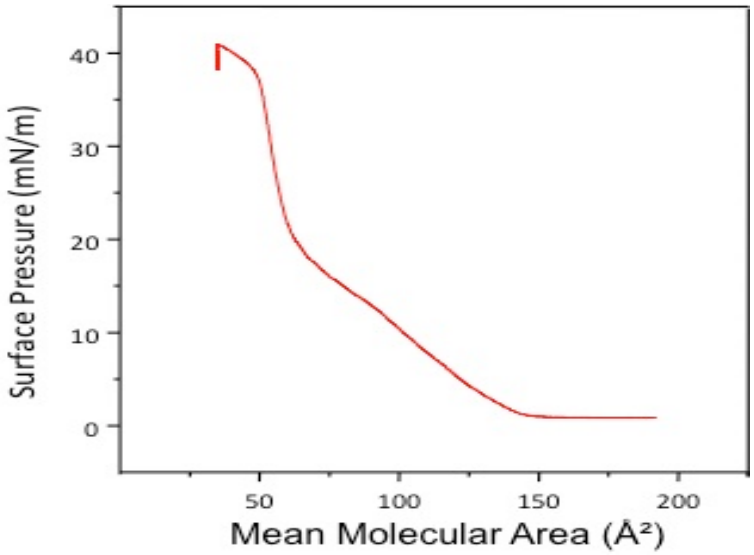

Figure 5.3 Surface pressures vs. mean molecular area (π-A) **isotherm**

5.2.2 Electronic absorption

Figure 5.4 shows the absorption spectra of 10^{-5} M solutions of *fluorescein DHPE* in chloroform with band maxima at around 451 and 492nm. For reference, the fluorescein absorption in chloroform with band maxima at around 430 and 450nm is also included. The extinction spectrum of the LB monolayer of *fluorescein DHPE* also shows broad absorption around 490nm. The absorption maximum is likely the result from the π-π* electronic transitions of the chromophore.

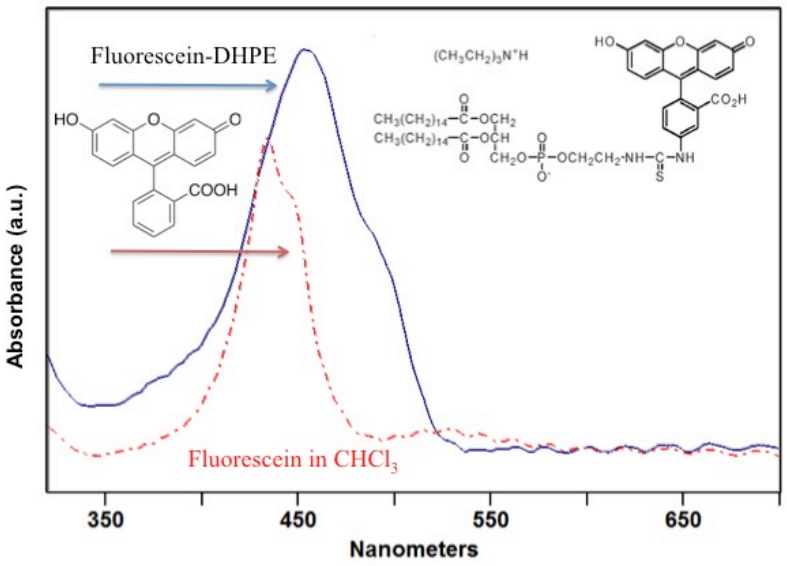

Figure 5.4 Extinction spectrum of fluorescein and fluorescein-DHPE in chloroform

Comparing the spectra shown in Figures 5.2 and 5.4, it can be seen that SIF exhibit a broad plasmon excitation in the visible range with a maximum around 420 nm, indicating a relatively large distribution of particle geometries and particle-particle interactions. Using the 514.5 nm laser excitation, it can be seen that it is in resonance with the localized surface plasmon resonance (LSPR) absorption of the SIF, (necessary condition for SERRS), and also with molecular electronic absorption of *fluorescein DHPE*, achieving the double-resonance. The AFM image for the morphology of 6 nm mass thickness film shows an inhomogeneous distribution of particles with sizes ranging between 40 and 80 nm (Figure 5.2).

5.2.3 Characteristic vibrational modes of the tagged phospholipid

Characteristic vibrational modes are vibrational bands observed in the Raman (or the infrared) which carry the largest Raman cross section (or absorption cross section in the infrared)[7]. The first step in this project is the vibrational characterization of the tagged phospholipid -tracking the phospholipid and the chromophore.

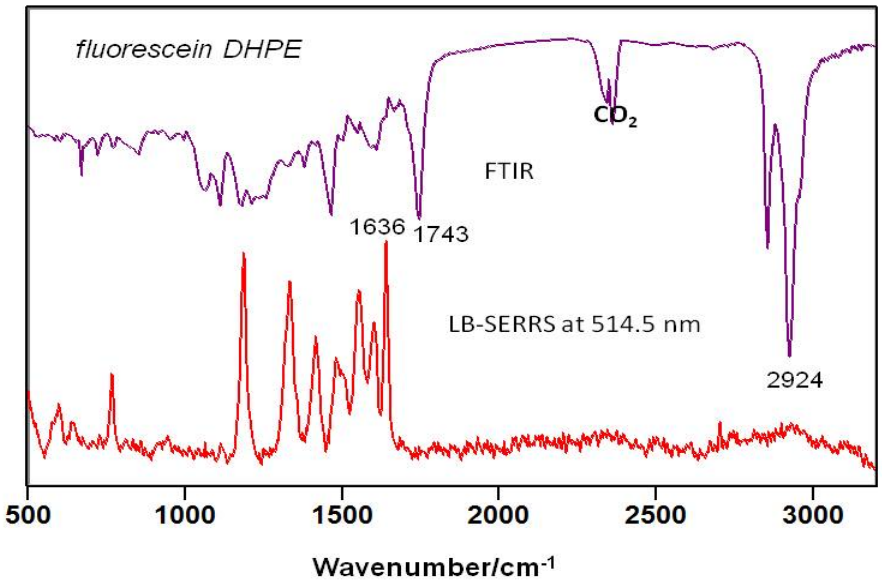

Figure 5.5 FTIR spectra for cast film of fluorescein-DHPE on Ge and LB-SERRS spectrum on SIF at 514.5 nm.

For comparison, the infrared and enhanced resonance-Raman spectra (using 514.5 nm) for *fluorescein DHPE* are shown in Figure 5.5. FTIR spectrum in transmission mode was collected from a cast film of *fluorescein DHPE* deposited onto a Ge plate. The infrared spectrum consists of vibrational bands from the phospholipid and the chromophore while The RRS spectrum is entirely from the vibrations of the chromophore. In the IR spectrum, the C-H stretching modes, which are the strongest bands, as same as the C=O stretching band at 1743 cm^{-1} (ester carbonyl group phospholipid)[57], are not observed in the RRS spectrum. On the other hand, in RRS

spectrum of *fluorescein DHPE*, the ring stretching of chromophore at 1636 cm^{-1} and 1328 cm^{-1} as some of the most intense bands. The SERRS *fluorescein DHPE* is not very different in relative intensities, in comparison with the spectra recorded with the 632.8 nm and 785 nm laser lines, as can be seen in Figure 5.6. Notably, the only laser line in full resonance with molecular electronic absorption given RRS is the 514.5 nm. That explains differences in the relative intensity of the characteristic vibrational bands, and it also explain the similarity between the spectra excited with the 632.8 nm and 785 nm laser lines.

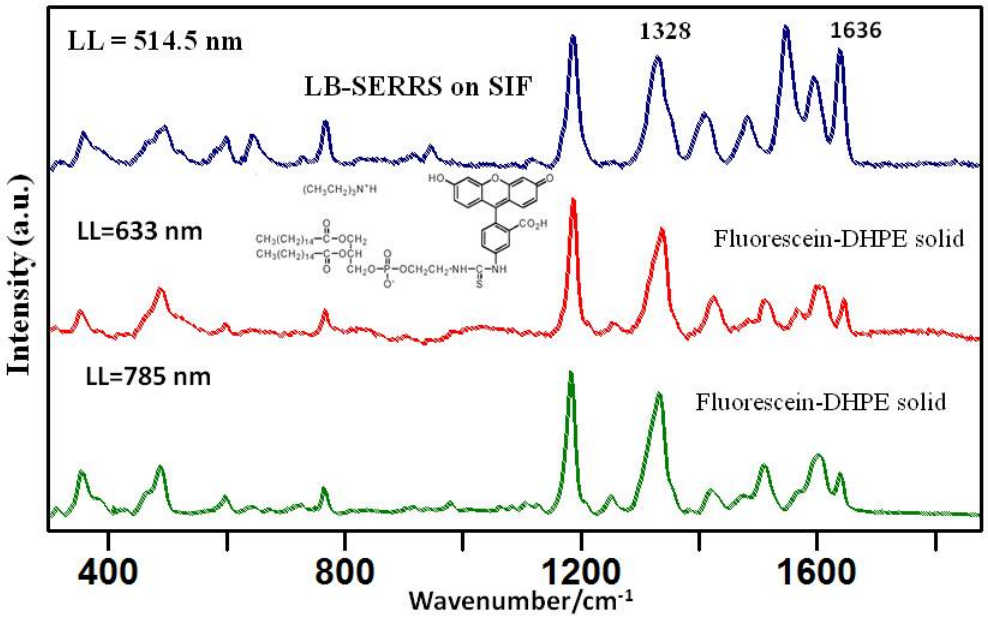

Figure 5.6 Raman spectra of *fluorescein DHPE* recorded with different laser lines

Characteristic vibrational modes of *fluorescein DHPE* are collected in Table 5.1. Notably the FTIR spectrum of the solid *fluorescein DHPE* contains molecular vibration of the phospholipid and the chromophore, while the RRS and the pre-resonant spectra

show mainly the molecular vibrations of the chromophore. The most intense bands in the infrared spectrum are due to the symmetric and anti-symmetric C-H stretching of the polymethylene chain of the lipid[58]. The carbonyl stretch is the most intense band in the IR of the low frequency region at 1742 cm^{-1}. Another characteristic lipid vibration is the C-C stretching mode seen at 1061 cm^{-1} [58]. These bands are not seen in the LB-SERRS and the tentative assignment is based on published work on phospholipids and related molecules.[59-61] To help the assignment of characteristic chromophore modes, we carry out a quantum mechanical calculation using Gaussian suite of programs, RB3LYP and the basis set 6-311+G (d, p). The proposed assignment for observed vibrations is given in Table 5.1

Table 5.1 Characteristic vibrational Raman modes and FTIR modes for F-DHPE

Experimental FTIR	*Experimental LB-SERRS*	*Vibrational Assignment*
	358 m	Anthracene ring deformation
	493 m	Ring deformation+N-H wag
	597 m	Benzene wagging
649 vw	645 m	Anthracene C-H wagging
677 w		CH_2 rocking
724 w	727 w	Benzene deformation
769 w	769 m	Anthracene ring breathing
776 w		O-P-O stretching
850 m		O-P-O stretching
952 w	947 w	C-N stretching asymmetric (head group - phospholipid)
1061 m		C-C Stretching phospholipid
1110 m		C-C Stretching phospholipid
1180 m	1183 vs.	C-H bending + O-H bending (in benzene ring)
1212 w		C-O stretching phospholipid
1260 w		CH_2 twist phospholipid
1328 vw	1328 vs	Anthracene ring stretching+ C-H bending
1378 w		CH_2 scissoring (chain phospholipid)
	1400 s	Benzene stretch + C-H bending + O-H bending
1465 m		CH_2 scissor (chain phospholipid)
	1483 s	Anthracene ring stretching)
1545 vw	1545 vs	Anthracene ring stretching
1591 sh	1591 s	Anthracene ring stretching
1636 sh	1636 vs	C=O and C=C ring stretching
1742 s		C=O stretching (phospholipid)
2852 s		Symmetric C-H stretching (phospholipid chain)
2872 sh		C-H Stretching
2924 vs		Antisymmetric C-H Stretching (phospholipid chain)
2953 sh		C-H Stretching

vs= very strong; s=strong; sh=shoulder; m=medium; w=weak

5.2.4 Single molecule detection

The sensitivity of LB-SERRS is reassuring to pursue dilution studies for single molecule detection. The LB-SERRS spectrum matches the reference spectra (including pre-resonance Raman scattering) indicating that the silver island films are not interacting chemically with the monolayers of tag-phospholipid, which means there is physical adsorption and the enhancement is plasmonic. The reference LB-SERRS spectrum is

exactly the same as the SERRS spectrum of *fluorescein DHPE* casted on silver island films as can be seen in Figure 5.7.

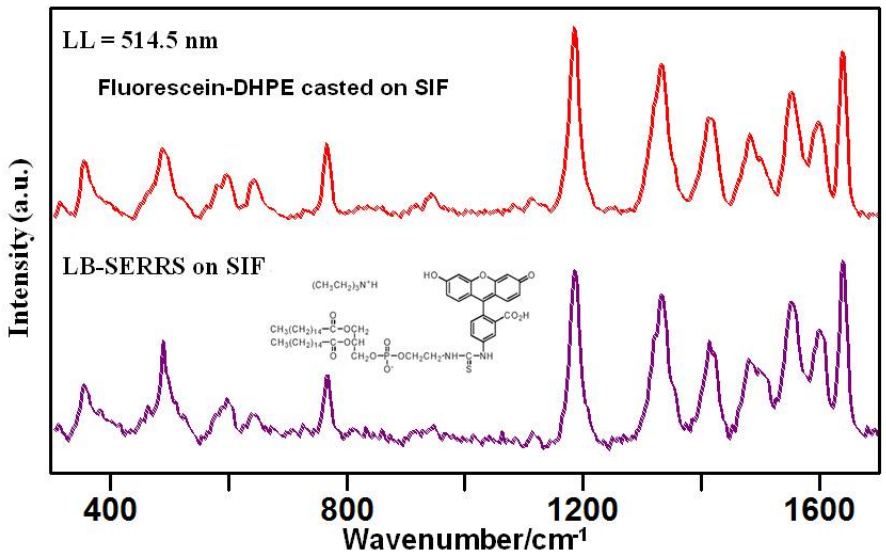

Figure 5.7 SERRS and LB-SERRS spectra of *fluorescein DHPE* on SIF

For ultrasensitive detection, different mixing ratio solutions leading to a few target molecules per 1μm^2 of surface area in the floating monolayer i.e. 10:3,999,990, 100:4,999,900, 1000:3,999,000 were prepared and transferred to SIF. The spectral data were recorded using point-by-point spectral mapping on LB films with 514 nm laser excitation. When we have, in average, ca. 10 target molecules per 1μm^2, using the signal to baseline mapping routine (Wire 3.4) on the intensity of 1636 cm^{-1} band for 2400 spectra, we only see a few reliable spectra that are most likely due to the detection of a single molecule as shown in Figure 5.8. It should be remember that SM detection is a rare event-taking place at the spatial locations where a molecule is located at a hot spot. It is assumed that only highly localized local fields or *hot spots*[41] are responsible for the observation of single molecule SERRS spectra. Figure 5.8 shows one LB-SERRS

reference and two single molecule spectra from the recorded data set. As it is common in the SM spectra[64], in the absence of the statistical average, minor changes in relative intensities and frequency shifts are observed form one SM spectrum to another.

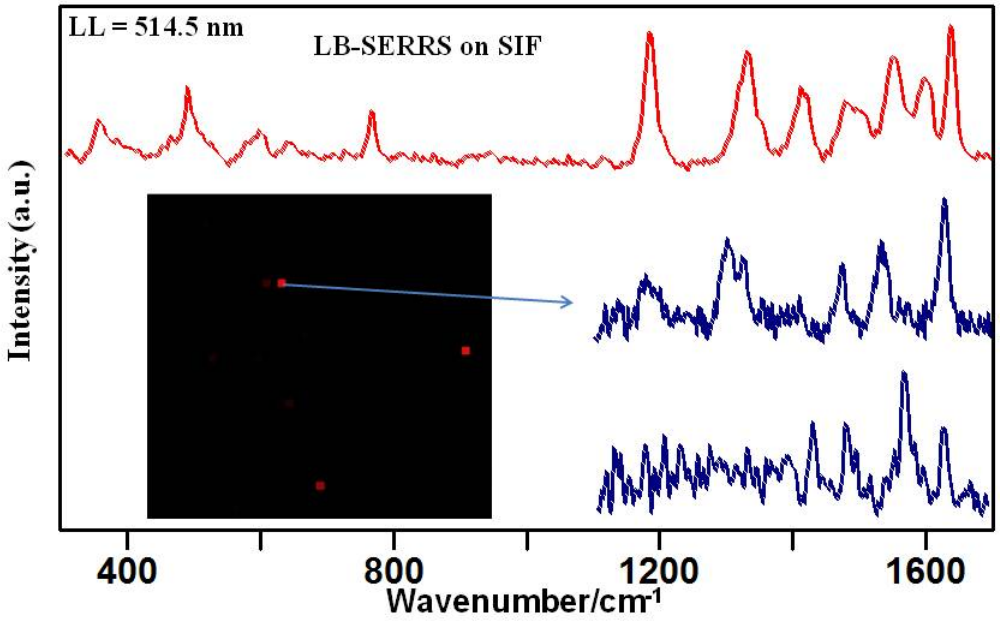

Figure 5.8 LB-SERRS spectra and mapping image for 10 target molecules per 1μm^2 of LB surface on SIF.

5.2.5 SHINEF from Fluorescein-DHPE

The SHINEF spectra of fluorescein-DHPE are obtained using Au-SHIN on an LB monolayer of the target molecule. Notably, the fluorophore has a high quantum yield ~0.95[24]. Fluorescein's extinction spectra as well as the comparable fluorescein-DHPE spectra are presented in Figure 5.9. The latter Figure includes the emission spectra of a solution of fluorescein-DHPE and a LB film that are the reference spectra. The fluorescence is collected excitating with the 514.5 nm laser line. The gold SHINs have a

plasmon peak is 524 nm (Figure 5.10) in tune with the emission of fluorescein-DHPE as shown in Figure 5.9**.**

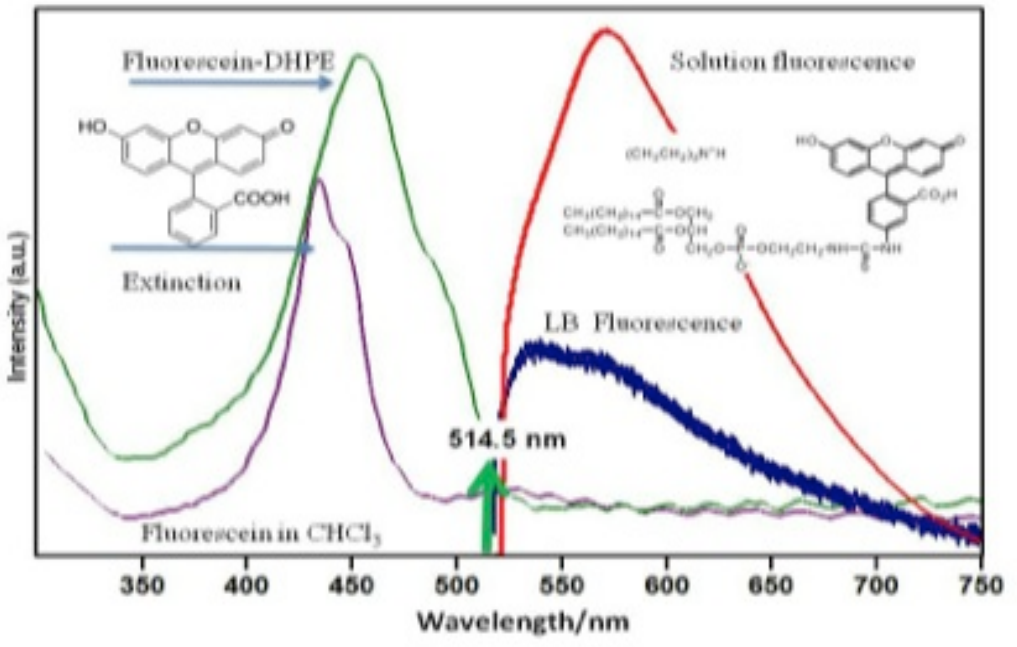

Figure 5.9 Extinction and emission spectra of fluorescein-DHPE, with the extinction spectrum of fluorescein also LB film

SHINEF measurements are carried out by casting Au-SHINs on a LB monolayer of fluorescein-DHPE molecules on quartz. The SHINEF that is observed with excitation fixed at 514.5 nm as shown in Figure 5.10. Since casting does not provide a uniform coverage, we record a spectral mapping ~108 spectra on the surface of the LB covered by SHINs. The highest enhancement factor so obtained was 68. The CCD camera reveals that EF maximum occurs within the spatial area where large SHIN particle aggregates seems to be formed.

In a separate experiment, a micro litre of gold SHINs is added to a fluorescein-DHPE in chloroform solution. The resulting fluorescence of the solution was monitored. A SHINEF enhancement of ca. 2 was attained. This is a rather small EF compared to those

from experiments that involve solid substrates. The enhancing nanoparticles that are present in solutions are in all probability separated-gold SHINs, i.e, they do not form aggregated nanostructures, as they do in the case of the solid substrate. Such an advantage of aggregation is comparable to the results presented for R18's experiments in a previous chapter.

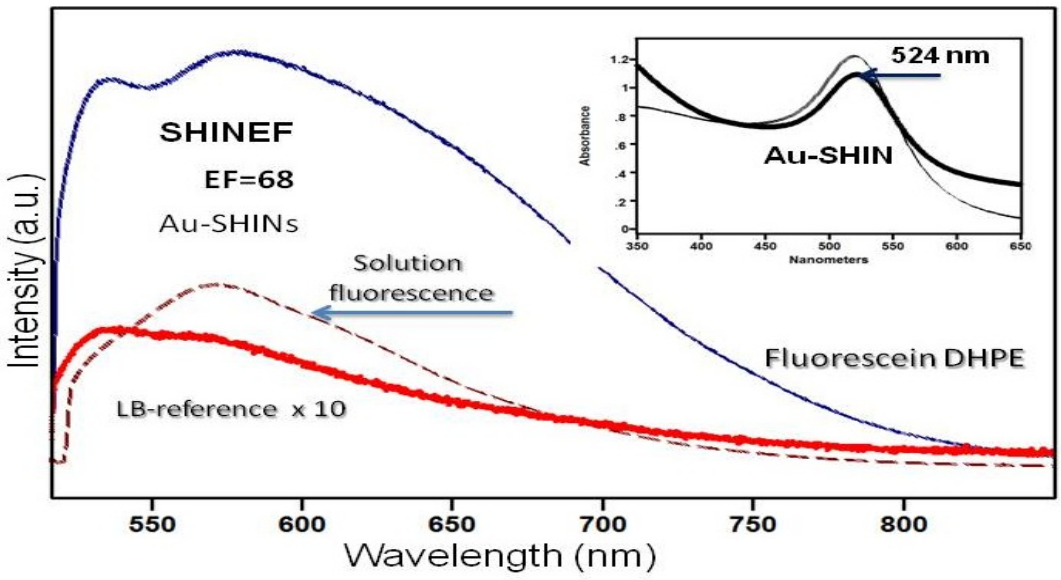

Figure 5.10 Plasmon enhanced fluorescence for fluorescein-DHPE with gold SHINs also LSPR of Au SHINs (bold line) and Au colloid (inset)

5.3 Conclusions

The plasmon enhanced scattering and fluorescence are illustrated in Langmuir-Blodgett films using fluorescein-DHPE tagged phospholipid as the target molecule. The molecular fingerprints observed in SERRS on silver island films may be used for ultrasensitive detection. Plasmon enhanced fluorescence (SHINEF) of a high quantum yield chromophore in LB films is achieved using gold shell isolated nanoparticles.

Chapter 6

Plasmon enhanced scattering and fluorescence of NBD tagged phospholipid

This project is an extension of our investigation of the plasmon enhancement of emission and scattering to a phospholipid covalently attached to 7-nitro-2-1,3-benzoxadiazol-4-yl (NBD) group, that has been extensively used to study the properties, spatial organization, and distribution of phospholipids and proteins in monolayers, bilayer, and biological membranes[65-68]. The NBD chromophore (7-nitro-2,1,3-benzoxadiazole or nitrobenzofurazan) may link to phospholipids to either the polar head group or to the apolar aliphatic chain of the phospholipid. Considering both of these orientations may help to monitor the changes in the photophysical behavior and gain important information about the phospholipid membrane such as aggregation, phase separation and other processes. Recent studies of NBD in organic solvents show that NBD display solvatochromic properties owing to the large dipole moment that may increase upon excitation[69]. The polar properties of NBD group might induce a looping back of the fluorescent moiety toward the membrane surface. In other word, the preference of the NBD to polar environment induces the looping NBD-acyl chain toward the aqueous phase.

The way that NBD is attached to the head group or aliphatic acyl chain produces different phospholipid properties. In our work 7-nitrobenz-2-oxa-1,3-diazol-4-yl(NBD) is attached to long chain fatty acid analog C12 (dodecanoyl) in sn2-position (see Figure 6.1). The isotherm shows liquid expanded behavior. Surface potential data and spectroscopic data illustrate that the NBD group is attached to the head group of the phospholipid looping the NBD labeled chain of C12-NBD-PC toward water. The less structured environment of NBD group on C12-NBD-PC allows the rotation of the NBD, also fast relaxation of water dipoles. Fluorescence quenching studies has been shown that

the rotation is due to the polarity of NBD group and the flexibility of the acyl chain. The dipole moment may be able to change between the ground and excited states probably due to reorientation in its excited state. Independent studies show that changing the polarity of the surrounding medium can control the quantum yield; this will dominate the rate constant of the nonradiative deactivation processes. Following the Demchak-Fort three layer capacitor model, which is used to give microscopic structural information, the surface potential ΔV results from the contribution of the dipole moments μ_i of aliphatic molecules of monolayer at air/water surface including the dipole moment of terminal CH_3 groups, hydrophilic head groups, and water molecules reoriented and polarized by the monolayer.[69]

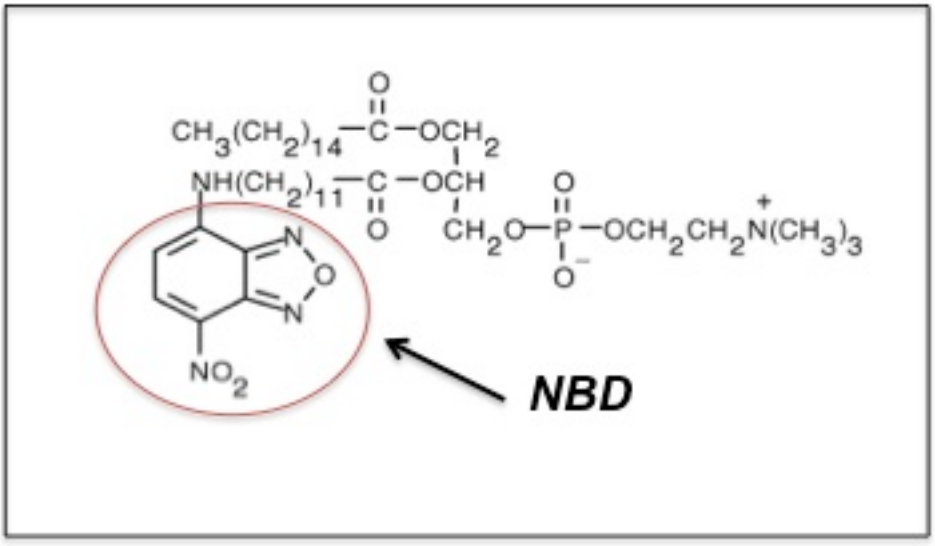

Figure 6.1 Illustration for chemical structures of the tag phospholipid

This chapter discusses the plasmon enhancement of emission and scattering using the LB technique to handle the molecular target. The enhanced fluorescence is attained using shell isolated nanoparticles, while SIF are used for surface enhanced resonance

Raman. The enhanced fluorescence of long chain alkylamine derivatives of nitrobenzoxadiazole (NBD-C16 and NBD-C18) deposited directly on SIF, using the Langmuir-Blodgett technique, has been reported [70]. It was shown that for the LB NBD monolayer deposited in close proximity to silver islands, a 16-fold increase in fluorescence intensity is possible.

The absorption cross section and the quantum yield are two factors should be considered when it comes to choose the fluorophore in tagged phospholipids.

$$P_0^{fluo} = k_0 I_0 Q_0 \qquad [6.1]$$

Where, k_0 is the absorption coefficient, I_0 is the photon flux impingent on the fluorophore and Q_0 is the quantum yield.

$$Q_0 = \frac{\Gamma_{rad}}{\Gamma_{rad}+\Gamma_{nR}} \qquad [6.2]$$

Where, Γ_{rad} is the radiative decay rate and Γ_{nR} is the non-radiative decay rate. The absorption rate of the fluorophore near the metallic nanoparticles will also be modified due to the local field of the excited surface plasmon and the total average enhancement factor (EF) will be represented by the ratio of the enhanced local field and the incident field[71, 72].

$$EF = \frac{|E_{loc}|^2}{|E_0|^2} \qquad [6.3]$$

Since I_0, the photon flux impingent on the fluorophore, is proportional to $|E_0|^2$, the emission enhancement is due to E_{loc}. However, when a chromophore is too close to

metallic nanoparticles strong quenching will take place[33]. As a result of the direct energy transfer to the metal, a new non-radiative decay channel is created.

$$Q_0 = \frac{\Gamma_{rad}}{\Gamma_{rad}+\Gamma_{nR}+\Gamma_{nR}^{metal}} \qquad [6.4]$$

Therefore, the distance dependence is a key factor and property of SEF[47, 73]. In this project we use a shell-isolated nanoparticles (SHINs) [74] to provide a molecule-metal separation system and avoid a fluorescence quenching. When the core gold or silver is coated with silica with thickness around 10 nm, the silica will give the needed stability as it offers a non-metallic surface for the interaction with fluorophores, and also protects the metal from surface reactions. In a typical SHINEF experiments, the SHINs will be casted over a LB monolayer deposited on glass or quartz (containing a tag-phospholipid)[45, 74].

In this work, Silver island films (SIF) of 6 nm mass thickness are used to obtain SERRS [4]. SERS experiments are attempted using colloidal gold generated by reducing the corresponding salt using trisodium citrate. The metal colloids fabricated by this established protocol provides metal nanoparticles with a surface that bears negative charges and the suspension of colloids is stable [75, 76].

6.1 Experimental

2-(12-(7-nitrobenz-2-oxa-1,3-diazol-4-yl)amino)dodecanoyl-1-hexadecanoyl-*sn*-glycero-3-phosphocholine C12-NBD-HPC was purchased from Invitrogen. Arachidic acid –(the saturated fatty acid with a 20 carbon chain- $CH_3\left(CH_2\right)_{18}COOH$), chloroform, and ultrapure (99.9%) Ag shot (1-3 mm) were obtained from Aldrich and used without

further purification. The spreading solution was prepared with HPLC chloroform and wrapped in aluminum and stored in freezer. The SHINs' synthesis using the method of[39] Li et al. was discussed in chapter 2.

SHINEF target samples were prepared using the LB technique; z-deposition at air/water interface. LB film with about 10^6 molecules of C12-NBD-HPC within $1\mu m^2$ over quartz slides. The same LB films were also transferred onto silver island films of 6 nm mass thickness and were used for SERRS work. The SIFs were vacuum evaporated onto Corning 2048 microscope glass slides.

UV-visible absorption spectra are recorded for tag-phospholipid, colloids, SHINs solutions and SIFs using a Cary 50 scan UV-Visible Spectrophotometer. Atomic Force Microscopy (AFM) images were recorded using a digital instruments NanoScope IV operating in tapping mode with an n^+ silicon tip. Renishaw InVia system with laser excitation at 514.5 and 633 nm using laser power of less than 1 mW, and a 50x microscope objective is employed for SHINEF, SERRS and SERS measurements. All the measurements were extended mapping and were collected through computer controlled stage. Data analysis was done using GRAMS software.

6.2 Results and Discussions

6.2.1 Absorption and resonance Raman scattering

The absorption spectra of neat C12-NBD-HPC solution and the plasmon absorption of silver island film are shown in Figure 6.2. The tag-phospholipid absorbed in the visible region due to the π-π^* electronic transition of the chromophore NBD from

the ground electronic state to any of the excited vibrational states, and the extinction spectrum shown in Figure 6.2 is in full agreement with reported spectra[70]. The SIF has a maximum at ca. 420 nm with a broad extinction spectrum covering the visible region, confirming a broad distribution of particle sizes and interactions between nanoparticles. A typical AFM image of 1μm^2 area of SIF is also shown using tapping mode. The morphology of AFM image shows the inhomogeneous distribution of particle sizes. The 514.5 nm laser excitation line is in resonance with plasmon absorption of SIF and the electronic absorption of C12-NBD-HPC with a maximum at 460 nm, achieving the double resonance condition (SERRS).

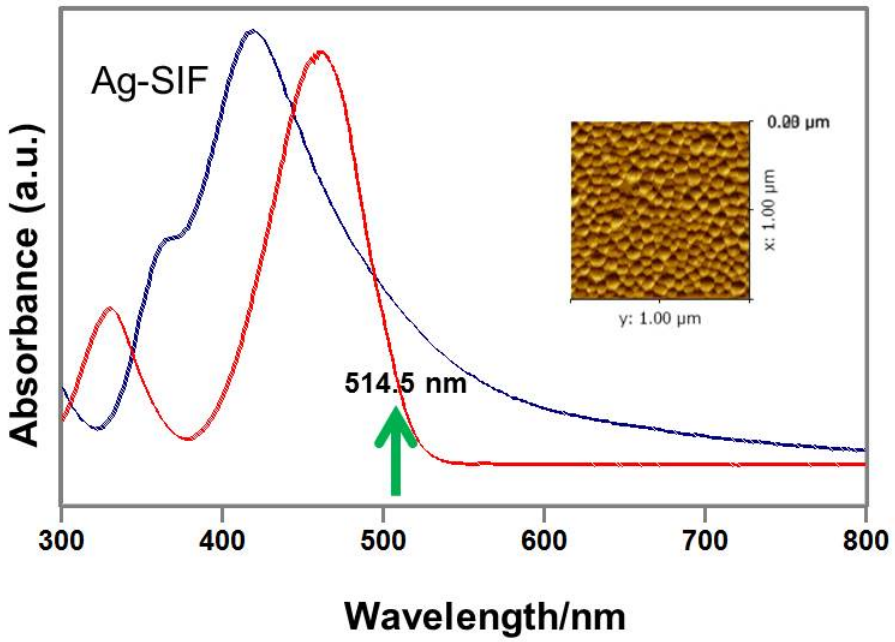

Figure 6.2 Extinction spectra of C12-NBD-HPC in solution and SIF. Inset, AFM of Ag island film.

Figure 6.3 shows the plasmon absorption of Au colloid and the electronic absorption of C12-NBD-HPC. It can be seen that the 632.8 nm laser line is outside the molecular electronic spectrum and can be used to explore SERS work. The extinction and fluorescence spectra of 10^{-4} C12-NBD-HPC solution are shown in Figure 6.4. The fluorescence spectrum of solution of C12-NBD-HPC is the mirror images of absorption, the 0-0 transition of C12-NBD-HPC appears at around 460 nm and emission peak was at 580 nm.

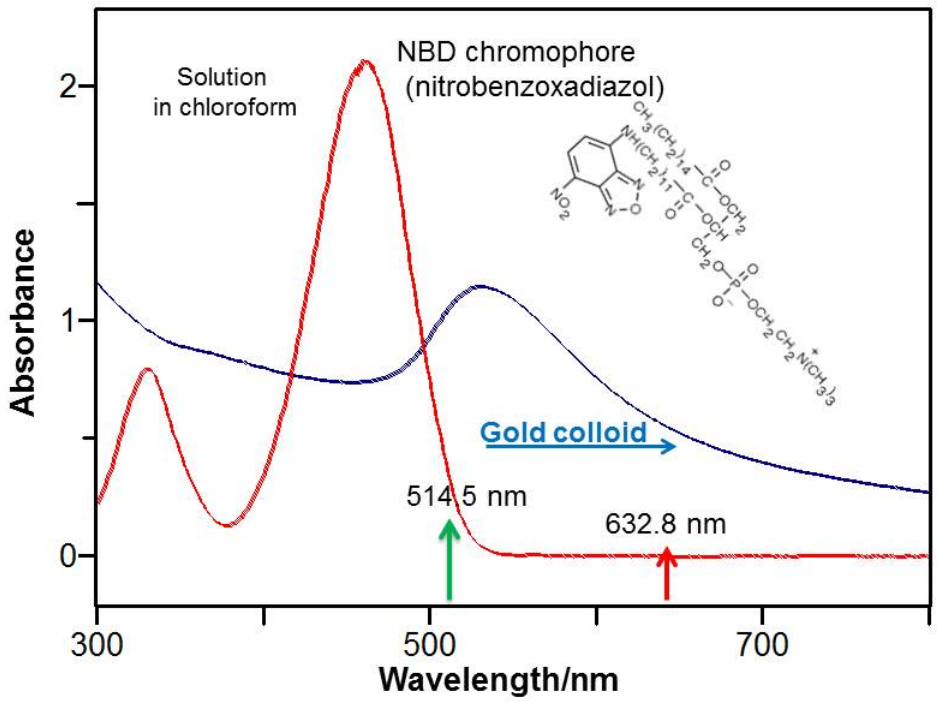

Figure 6.3 Extinction spectra of C12-NBD-HPC in solution and Au colloidal solution.

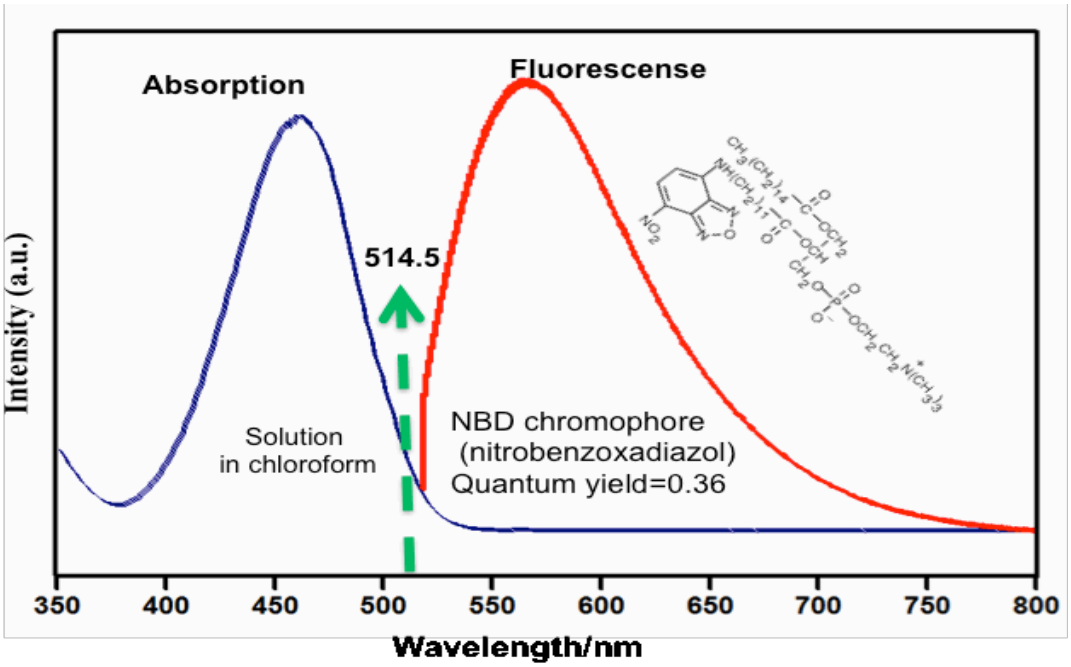

Figure 6.4 Extinction and fluorescence spectra of 10^{-4} M C12-NBD-HPC solution

The surface-pressure area isotherm was recorded spreading a solution of C12-NBD-HPC in chloroform on water surface at room temperature. The surface-area isotherm of neat C12-NBD-HPC exhibits two-phase transitions: a gas-liquid transition and condensed phase. The molecules at air water interface are likely organized, where the hydrophobic part is away from the water surface and polar part is toward the water surface. The monolayer was held at a constant surface pressure of 25 mNn/m and transfer to solid substrates (silver island film or quartz slides).

6.2.2 Average SERRS spectra

LB monolayer of C12-NBD-HPC fabricated on silver island film was used to obtain enhanced resonance Raman scattering exciting at 514.5 nm using and collecting extended mapping. Figure 6.5 shows the average LB-SERRS spectra and Raman spectrum of the solid sample of the phospholipid. The comparison demonstrates that the

LB-SERRS spectrum is entirely due to the chromophore, i.e., the fundamentals vibrational modes of NBD chromophore are observed. As can be seen the C=O and CH stretching bands are absent in the LB-SERRS spectra. Since the most intense bands (stretching bands) are absent, any other vibrational mode of the phospholipid will be very weak in LB-SERRS spectrum. To further illustrate the idea, another comparison between the LB-SERRS of the tag-phospholipid and a simple fatty acid (Arachidic acid) is presented in Figure 6.6.

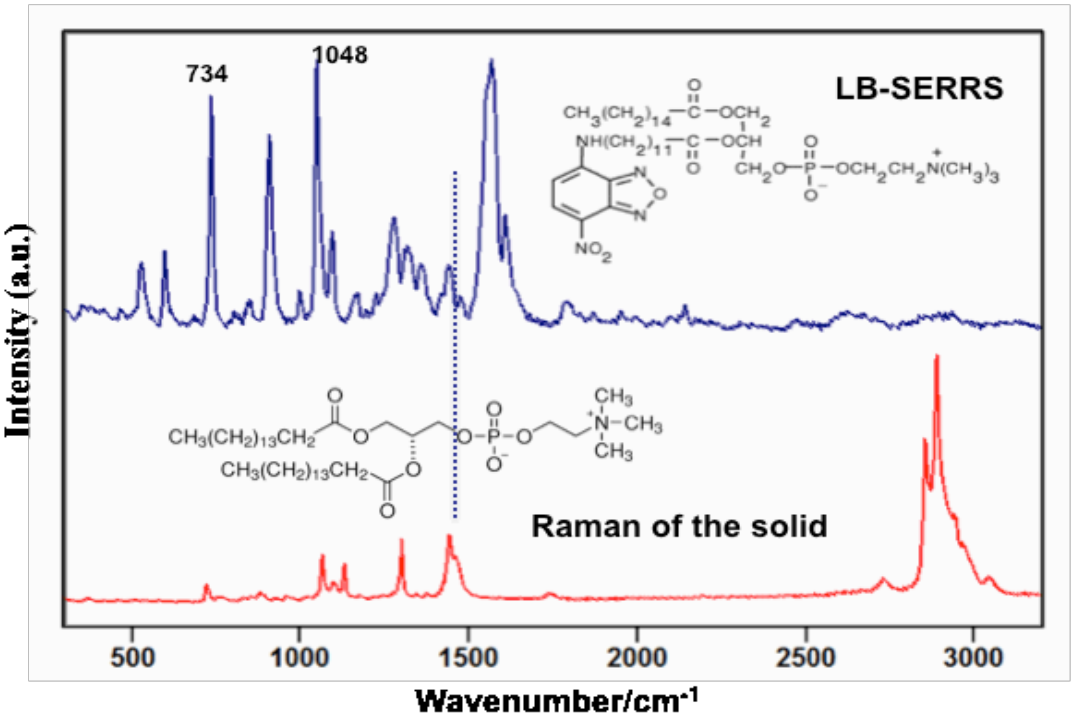

Figure 6.5 LB-SERRS of neat C12-NBD-HPC with Raman spectra of the solid phospholipid

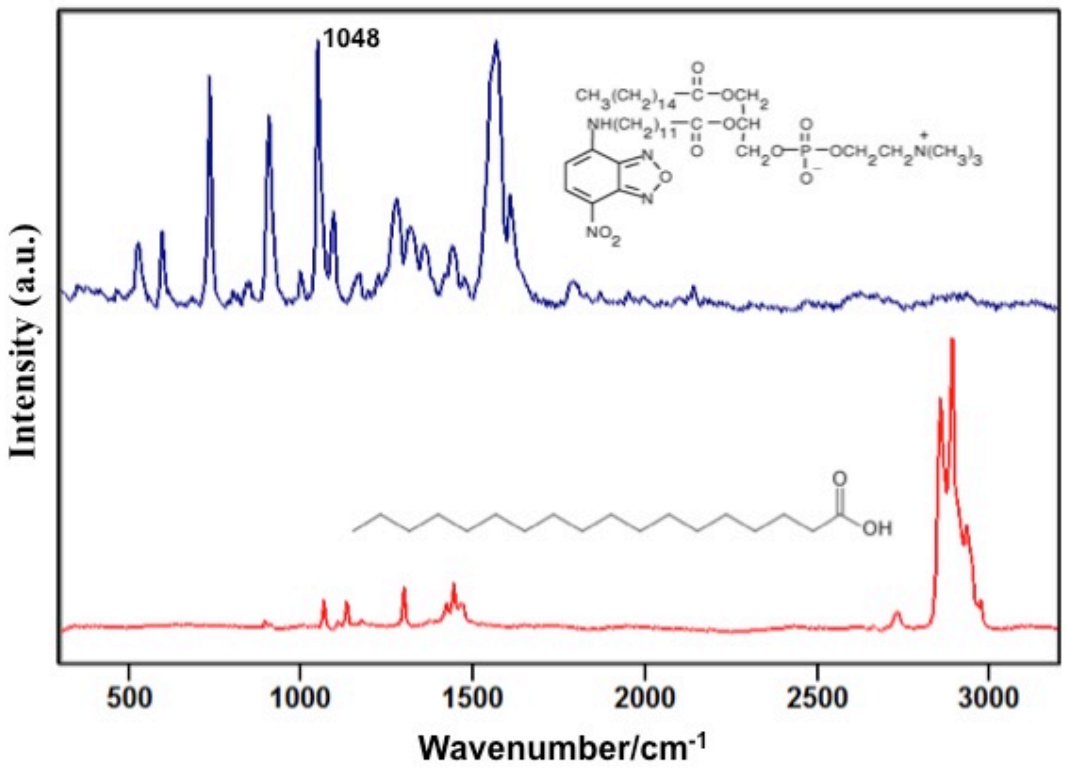

Figure 6.6 LB-SERRS of neat C12-NBD-HPC with Raman spectra of the fatty acid (Arachidic acid)

Therefore the vibrational modes seen in LB-SERRS in Figures 6.5 or 6.6 correspond to vibrational spectrum of the chromophore (4-amino-7-nitrobenzofurazan or NBD-amino). A complete vibrational analysis of 4-chloro-7-nitrobenzofurazan (NBD-Chloride) has been published recently[77] and it is used here to help the assignment of the characteristic modes observed in LB-SERRS. The vibrational wavenumbers with noticeable Raman intensities are collected in Table 6.1.

The strongest Raman bands correspond to the in-plane modes of the 7-nitrobenzofurazan ring. The band at 1561 cm^{-1} is an in-plane stretching mode of the nitrobenfurazan ring. In fact all the modes in this spectral region have perceptible contributions from the ring stretches[77]. Despite the quantity of C-Hs in the NBD phospholipid, the stretching C-H

is not seen in the LB- SERRS (see Figure 6.5). However, the in-plane CC–H bending vibrations that in the substituted benzenes appear in the range 1300–1000 cm^{-1} are seen with medium weak relative intensity at 1360 cm^{-1} and 1276 cm^{-1}.

The characteristics group frequencies of the nitro group (-NO_2) are relatively independent of the rest of the molecule, which makes this group easy to identify The nitro group attached to aromatic rings present a set of characteristic vibrations[78] in the 1400 cm^{-1} region (1440 cm^{-1} and 1319 cm^{-1}) for the stretching modes, a bending at 597 cm^{-1} and a rocking mode at 527 cm^{-1}. The out-of-plane modes, wagging and twisting, induce a minor change in the polarizability and carry very little intensity in the Raman spectrum.

Collective ring vibrations (breathing mode in benzene); normally are the most intense Raman bands in aromatic molecules. The actual position of these modes is determined by the nature of the substituents and the form of substitution around the ring. The CCC in plane ring breathing vibrations are observed at 1048 cm^{-1} and 734 cm^{-1} with strong Raman intensity.

The identification of C–N vibration in C-NO_2 is difficult because of the mixing of several modes. In the case of benzotriazole, the C–N stretching bands are found to be at 1307 and 1382 cm−1. However, the C-N stretch is seen in the 920-830 cm^{-1} range (Lambert page 172)[78], and we assigned the band at 907 cm^{-1} to this vibrations mode with strong ring mixing.

Table 6.1 Characteristic vibrational Raman modes in the LB-SERRS of neat C12-NBD-HPC

Observed wavenumber	Interpretation
1607 medium	C=C stretch
1561 very strong	Nitrobenzofurazan ring stretch
1440 weak	NO_2 stretching +furazan ring stretch
1360 weak	CC-H bending
1319 weak	NO_2 stretching +CC-H bending
1276 medium	CC-H bending
1092 medium	N-O-N stretch furazan ring
1048 very strong	Benzene ring breathing
999 weak	Furazan ring stretch
907 strong	C-N stretch + ring stretch
734 strong	Ring breathing
597 medium	NO_2 scissoring
527 medium	NO_2 rocking

Au colloids (before coating with SiO_2) were casted onto the monolayer of neat LB of C12-NBD-HPC. Excitation with the 514.5 nm laser line carries a strong fluorescence background. However, excitation with 633 nm laser line gave spectra that may be classified as surface enhanced Raman scattering due to plasmon enhancement. Since, the Au colloid is delivered by transferring a drop of it into the monolayer, these ere casted

colloids, only a few spots (points in the spectral map) produce spectra and is not recommended as an analytical tool. A typical surface enhanced Raman scattering spectrum obtained with 633 nm is shown in Figure 6.7 The latter spectrum contains vibrational modes of the NBD phospholipid, and not only those of the chromophore, as can besee by comparing Figures 6.5 and 6.7.

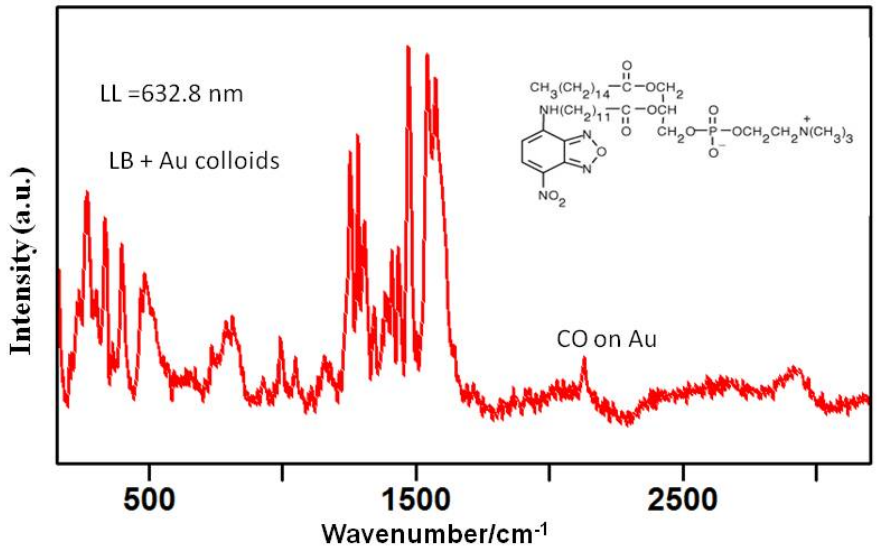

Figure 6.7 LB-SERS of neat C12-NBD-HPC LB with Au colloid

6.2.3 SHINEF in concentrated LB films

Fluorescence spectra of the same LB monolayer in with and without Au SHINs using a 514.5 nm laser excitation are shown in Figure 6.8. The emission from neat C12-NBD-HPC LB monolayer on quartz is recorded first and is the used as reference. It is marked as LB reference in Figure 6.8, and its intensity has been multiplied by a factor of 10, to facilitate visual comparison. The dame neat LB-monolayer is covered with gold shell isolated nanoparticles Au-SHINs, to compare the measured intensities with respect

to the reference. All the experimental variables are kept constant: laser power, microscope objective and acquisition times. The laser line 514.5 nm is in resonance with both the molecular electronic absorption and the au-SHIN plasmon resonance. Since the cast Au-SHINs cover a large space, a mapping of the fluorescence is recorded, and the highest intensity in the map was selected and shown in Figure 6.8. The enhanced fluorescence corresponds to monomer fluorescence, which is characteristic of C12-NBD-HPC and the best enhancement factor is 20.

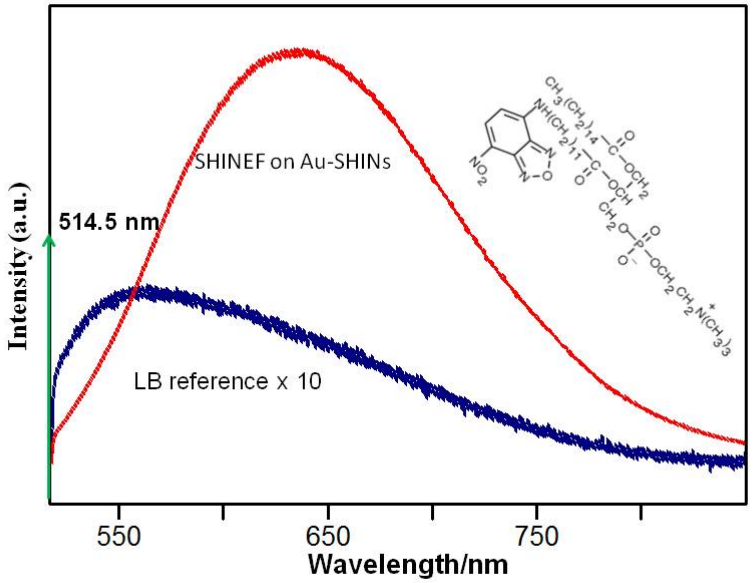

Figure 6.8 SHINEF of neat C12-NBD-HPC LB in absent and in present of Au SHINs

6.3 Conclusion

Monolayer of neat C12-NBD-HPC was transferred at air-water interface onto SIF and quartz slides. SERRS spectra were obtained with reproducible results using the 514 nm

laser line excitation, and this analytical protocol is recommended for NBD phospholipid detection. The reproducible results from LB-SERRS allow characterizing the tag-phospholipid. LB-SERS is also detected with Au colloid using the 633 nm laser line excitation. Using shell isolated nanoparticles LB-SHINEF is demonstrated with an enhancement factor off about 20 providing an analytical technique for ultrasensitive detection tag-phospholipids.

Chapter 7

Conclusions

7.1 Conclusions

In this thesis we have examined different spectroscopic analytical techniques, in particular, surface-enhanced resonance Raman scattering (SERRS) and shell isolated nanoparticle enhanced fluorescence (SHINEF). Therefore, we fabricate SERS/SERRS substrates with silver and gold nanoparticles, and the target molecules are manipulated using Langmuir-Blodgett monolayer. The enhanced fluorescence of tagged phospholipids is reported using Langmuir-Blodgett technique and gold core coated with SiO_2.

In chapter 4, the fabrication of self-assembly SHINEF substrates (Ag SHINs) is reported. SHINEF is tested with neat LB monolayers of octadecyl rhodamine B chloride R18. The enhancement factor of the substrate was proportional to the time of deposition, due to the growth of the nanoparticle aggregates.

In chapter 5, the LB-SERRS spectra of dye-tagged phospholipid (F-DHPE) in LB monolayer on silver island films is presented. The highest SERRS enhancement may be used for ultrasensitive detection, We use fluorescein dye tag, with high quantum yield value, and Au-SHINs to obtain SHINEF.

Finally, the chapter 6 carried out the same SHINEF work using a low quantum yield tag. Gold SHINs are used experimentally to enhance the fluorescence emission. Ultrasensitive detection using silver island films to achieve SERRS is demonstrated.

7.2 Future work

The SHINs play an important rule in the analytical enhanced spectroscopy. Base in the need of SHINs particles we are investigating new coated particles for SHINERS-SHINEF applications. Gold or silver core are coated with permanganate, which can control experimentally. Furthermore, this is a great challenge to obtain hot spots with controllable aggregation. In addition, this may present model to explain the enhancement factor in this thesis.

References

1. Herzberg, G., *Molecular Spectra and Molecular Structure. I Spectra of Diatomic Molecules.* 2nd. ed1950, Princeton, N.J.: D.Van Nostrand Co., Inc.
2. Herzberg, G., *Molecular Spectra and Molecular Structure. III Electronic Spectra and Electronic Structure of Polyatomic Molecules*1966, Princeton, N.J.. D. Van Nostrand Co., Inc.
3. Long, D.A., *The Raman Effect. A unified treatment of the theory of Raman scattering by molecules*2001, Chichester: John Wiley & Sons, Ltd.
4. Aroca, R., *Surface-enhanced Vibrational Spectroscopy* 2006, Chichester: John Wiley & Sons.
5. Le Ru, E.C. and P.G. Etchegoin, *Principles of Surface Enhanced Raman Spectroscopy (and related plasmonic effects)*2009., Amsterdam: Elsevier.
6. McCreery, R.L., *Raman spectroscopy for chemical analysis*. 3rd ed2000, New York: Wiley-Interscience.
7. Wilson Jr, E.B., J.C. Decius, and P.C. Cross, *Molecular Vibrations; The Theory Of Infrared And Raman Vibrational Spectra*1955, New York: McGraw-Hill.
8. Garrell, R.L., *Surface-Enhanced Raman-Spectroscopy.* Analytical Chemistry, 1989. **61**(6): p. A401-A411.
9. Kneipp, K., et al., *Ultrasensitive chemical analysis by Raman spectroscopy.* Chemical Reviews, 1999. **99**(10): p. 2957-2975.
10. Maier, S.A., *Plasmonics: Fundamentals and Applications* 2007, New York: Springer.

11. Jeanmaire, D.L. and R.P. Van Duyne, *Surface Raman spectroelectrochemistry. Part I. Heterocyclic, aromatic, and aliphatic amines adsorbed on the anodized silver electrode.* Journal of Electroanalytical Chemistry and Interfacial Electrochemistry, 1977. **84**(1): p. 1-20.

12. Moskovits, M., *Surface-enhanced spectroscopy.* Reviews of Modern Physics, 1985. **57**(3): p. 783-826.

13. Meyer, S.A., E.C. Le Ru, and P.G. Etchegoin, *Quantifying Resonant Raman Cross Sections with SERS.* Journal of Physical Chemistry A, 2010. **114**(17): p. 5515-5519.

14. Pettinger, B., et al., *Tip-Enhanced Raman Spectroscopy: Near-Fields Acting on a Few Molecules*, in *Annual Review of Physical Chemistry, Vol 63*, M.A. Johnson and T.J. Martinez, Editors. 2012. p. 379-399.

15. Schatz, G.C. and R.P. Van Duyne, *Electromagnetic mechanism of surface-enhanced spectroscopy*, in *Handbook of Vibrational Spectroscopy*, J.M.C.a.P.R. Griffiths, Editor 2002, John Wiley & Sons, Ltd. p. 759-774.

16. Rubim, J.C. and R.F. Aroca, *The observation of high order overtones and combinations in the SERRS spectra of a perylene dye spin coated onto silver island films.* Physical Chemistry Chemical Physics, 2008. **10**(35): p. 5412-5418.

17. Willets, K.A. and R.P. Van Duyne, *Localized surface plasmon resonance spectroscopy and sensing.* Annual Review of Physical Chemistry, 2007. **58**: p. 267-297.

18. Kneipp, K., et al., *Single Molecule Detection using Surface-Enhanced Raman Scattering.* Phys. Rev. Lett., 1997. **78**: p. 1667-1670.

19. Nie, S. and S.R. Emory, *Probing single molecules and single nanoparticles by surface-enhanced Raman scattering.* Science (Washington, D. C.), 1997. **275**(5303): p. 1102-1106.

20. Moerner, W.E., *A dozen years of single-molecule spectroscopy in physics, chemistry, and biophysics.* Journal of Physical Chemistry B, 2002. **106**(5): p. 910-927.

21. Lee, S.J., A.R. Morrill, and M. Moskovits, *Hot spots in silver nanowire bundles for surface-enhanced Raman spectroscopy.* Journal of the American Chemical Society, 2006. **128**(7): p. 2200-2201.

22. Stranahan, S.M. and K.A. Willets, *Super-resolution Optical Imaging of Single-Molecule SERS Hot Spots.* Nano Letters, 2010. **10**(9): p. 3777-3784.

23. Pieczonka, N.P.W. and R.F. Aroca, *Inherent complexities of trace detection by surface-enhanced Raman scattering.* ChemPhysChem, 2005. **6**(12): p. 2473-2484.

24. Lakowicz, J.R., *Principles of Fluorescence Spectroscopy*. Third Edition ed2006, Singapore: Springer Science.

25. Jablonski, A., *Über den Mechanisms des Photolumineszenz von Farbstoffphosphoren.* Z. Phys., 1935. **94**: p. 38-46.

26. Brouwer, A.M., *Standards for photoluminescence quantum yield measurements in solution (IUPAC Technical Report).* Pure Appl. Chem, 2011. **83**(12): p. 2213-2228.

27. Moskovits, M., *Surface-roughness and enhanced intensity of Raman-scattering by molecules adsorbed on metals.* Journal of Chemical Physics, 1978. **69**(9): p. 4159-4161.

28. Mie, G., *Contributions to the Optics of Turbid Media, Especially Colloidal Metal Solutions.* . Annalen der Physik, 1908. **25**: p. 377-445.

29. Moula, G., et al., *Plasmonics and single-molecule detection in evaporated silver-island films.* Annalen Der Physik, 2012. **524**(11): p. 697-704.

30. Chance, R.R., A. Prock, and R. Silbey, *Molecular fluorescence and energy transfer near interfaces.* Advances in Chemical Physics, 1978. **37**: p. 1-65.

31. Sun, G., J.B. Khurgin, and D.P. Tsai, *Comparative analysis of photoluminescence and Raman enhancement by metal nanoparticles.* Opt. Lett., 2012. **37**(9): p. 1583-1585.

32. Sun, G. and J.B. Khurgin, *Origin of giant difference between fluorescence, resonance, and nonresonance Raman scattering enhancement by surface plasmons.* Physical Review A, 2012. **85**(6): p. 063410.

33. R. R. Chance, A.P.a.R.S., *Molecular fluorescence and energy transfer near metal interfaces.* Advances in Chemical Physics, 1978. **37**: p. 1-65.

34. Petty, M.C., *Langmuir-Blodgett Films: An Introduction*1996, Cambridge: Cambridge University Press.

35. Roberts, G., *Langmuir-Blodgett Films*1990, New York: Plenum Press.

36. Ulman, A., *An Introduction to Ultrathin Organic Films: from Langmuir-Blodgett to Self-Assembly*1991, San Diego: Academic Press, Inc.

37. Alessio, P., et al., *Surface-enhanced Raman scattering: metal nanostructures coated with Langmuir-Blodgett films.* Journal of the Chilean Chemical Society, 2011. **55**(4): p. 469-478.

38. Smith, D.L., *Thin-Film Deposition. Principles & Practice*1995, New York: McGraw-Hill, Inc.

39. Li, J.F., et al., *Shell-isolated nanoparticle-enhanced Raman spectroscopy.* Nature, 2010. **464**(7287): p. 392-395.

40. Chen, J.C., *Introduction to Scanning Tunneling Microscopy*. Oxfod series in optical and imaging sciences1993, New York: Oxford University Press.

41. Cang, H., et al., *Probing the electromagnetic field of a 15-nanometre hotspot by single molecule imaging.* Nature, 2011. **469**(7330): p. 385-389.

42. Xu, H., et al., *Spectroscopy of single hemoglobin molecules by surface enhanced Raman scattering* Physical Review Letters, 1999. **83**(21): p. 4357- 4360.

43. Fan, M., G.F.S. Andrade, and A.G. Brolo, *A review on the fabrication of substrates for surface enhanced Raman spectroscopy and their applications in analytical chemistry.* Analytica Chimica Acta, 2011. **693**(1-2): p. 7-25.

44. Gill, R. and E.C. Le Ru, *Fluorescence enhancement at hot-spots: the case of Ag nanoparticle aggregates.* Physical Chemistry Chemical Physics, 2011. **13**(36): p. 16366-16372.

45. Guerrero, A.R. and R.F. Aroca, *Surface-enhanced fluorescence with shell-isolated nanoparticles (SHINEF).* Angewandte Chemie (International ed. in English), 2011. **50**(3): p. 665-8.

46. Geddes, C.D.a.L., J.R., *Metal-enhanced fluorescence.* Journal of Fluorescence, 2002. **12(2)**: p. 121-129.

47. Wokaun, A., et al., *Energy transfer in surface enhanced luminescence.* Journal of Chemical Physics, 1983. **79**(1): p. 509-14.

48. Guerrero, A.R., Zhang, Y. & Aroca, R. F., *Experimental Confirmation of Local Field Enhancement Determining Far-Field Measurements with Shell-Isolated Silver Nanoparticles.* small, 2012. **8**: p. 2964-2967.

49. Mowald, H., *Surfactant layers at water interfaces.* Reports on Progress in Physics, 1993. **56**(5): p. 653-685.

50. Benda, A., et al., *Fluorescence lifetime correlation spectroscopy combined with lifetime tuning: New perspectives in supported phospholipid bilayer research.* Langmuir, 2006. **22**(23): p. 9580-9585.

51. Sabatte, G., et al., *Comparison of surface-enhanced resonance Raman scattering and fluorescence for detection of a labeled antibody.* Analytical chemistry, 2008. **80**(7): p. 2351-2356.

52. Faulds, K., et al., *Quantitative simultaneous multianalyte detection of DNA by dual-wavelength surface-enhanced resonance Raman scattering.* Angewandte Chemie-International Edition, 2007. **46**(11): p. 1829-1831.

53. Moula, G. and R.F. Aroca, *Plasmon-enhanced resonance Raman scattering and fluorescence in Langmuir-Blodgett monolayers.* Analytical chemistry, 2011. **83**(1): p. 284-8.

54. Pieczonka, N.P.W., G. Moula, and R.F. Aroca, *SERRS for Single-Molecule Detection of Dye-Labeled Phospholipids in Langmuir-Blodgett Monolayers.* Langmuir, 2009. **25**(19): p. 11261-11264.

55. Jensen, L. and G.C. Schatz, *Resonance Raman Scattering of Rhodamine 6G as Calculated Using Time-Dependent Density Functional Theory.* Journal of Physical Chemistry A, 2006. **110**(18): p. 5973-5977.

56. Le Ru, E.C. and P.G. Etchegoin, *Rigorous justification of the |E|4 enhancement factor in Surface Enhanced Raman Spectroscopy.* Chemical Physics Letters, 2006. **423**(1-3): p. 63-66.

57. Le Ru EC, S.L., Etchegoin PG., *Direct measurement of resonance Raman spectra and cross sections by a polarization difference technique.* 2012. **84**: p. 5074-5079.

58. Shimanouchi, T., *Tables of molecular vibrational frequencies. Consolidated volume I.*1972: Nat. Stad. Ref. Data Ser.,Nat. Bur. Stand. (US).

59. Ravikumar, B., R.K. Rajaram, and V. Ramakrishnan, *Raman and IR spectral studies of L-phenylalanine L-phenylalaninium dihydrogenphosphate and DL-phenylalaninium dihydrogenphosphate.* Journal of Raman Spectroscopy, 2006. **37**(5): p. 597-605.

60. Fowler, B.O., M. Markovic, and W.E. Brown, *Octacalcium phosphate. 3. Infrared and Raman vibrational spectra.* Chemistry of Materials, 1993. **5**(10): p. 1417-23.

61. Lin, S.-Y., M.-J. Li, and W.-T. Cheng, *FT-IR and Raman vibrational microspectroscopies used for spectral biodiagnosis of human tissues.* Spectroscopy (Amsterdam, Netherlands), 2007. **21**(1): p. 1-30.

62. Xu, H., et al., *Spectroscopy of single hemoglobin molecules by surface enhanced Raman scattering.* Phys. Rev. Lett., 1999. **83**(21): p. 4357-4360.

63. Michaels, A.M., J. Jiang, and L. Brus, *Ag Nanocrystal Junctions as the Site for Surface-Enhanced Raman Scattering of Single Rhodamine 6G Molecules.* J. Phys. Chem. B, 2000. **104**(50): p. 11965-11971.

64. Goulet, P.J.G. and R.F. Aroca, *Distinguishing individual vibrational fingerprints: Single-molecule surface-enhanced resonance Raman scattering from one-to-one binary mixtures in Langmuir-Blodgett monolayers.* Analytical Chemistry 2007. **79**(7): p. 2728-2734.

65. Garrett, F.E., et al., *Liposomes fuse with sperm cells and induce activation by delivery of impermeant agents.* Biochimica Et Biophysica Acta-Biomembranes, 1999. **1417**(1): p. 77-88.

66. Smriti, et al., *ABC transporters Cdr1p, Cdr2p and Cdr3p of a human pathogen Candida albicans are general phospholipid translocators.* Yeast, 2002. **19**(4): p. 303-318.

67. Morelli, J.K., et al., *Validation of an in vitro screen for phospholipidosis using a high-content biology platform.* Cell Biology and Toxicology, 2006. **22**(1): p. 15-27.

68. Eckford, P.D.W. and F.J. Sharom, *The reconstituted Escherichia coli MsbA protein displays lipid flippase activity.* Biochemical Journal, 2010. **429**: p. 195-203.

69. Mukherjee, S., et al., *Dipole-moment change of NBD group upon excitation studied using solvatochromic and quantum-chemical approaches - implications in membrane research.* Journal of Physical Chemistry, 1994. **98**(11): p. 2809-2812.

70. Ray, K., R. Badugu, and J.R. Lakowicz, *Langmuir-Blodgett monolayers of long-chain NBD derivatives on silver island films: Well-organized probe layer for the metal-enhanced fluorescence studies.* Journal of Physical Chemistry B, 2006. **110**(27): p. 13499-13507.

71. Gersten, J.N., A. , *Spectroscopic properties of molecules interacting with small dielectric particles.* Journal of Chemical Physics, 1981. **75**(3): p. 1139-1152.

72. Guerrero, A.R., Y. Zhang, and R.F. Aroca, *Experimental Confirmation of Local Field Enhancement Determining Far-Field Measurements with Shell-Isolated Silver Nanoparticles.* Small, 2012. **8**(19): p. 2964-2967.

73. R. Aroca, G.J.K., C. A. Jennings, R. o. Loutfy, and P. S. Vincett, *Fluorescence Enhancement from Langmuir-Blodgett Monolayers on Silver Island Films.* Langmuir, 1988. **4**(3): p. 518-521.

74. Li, J.H., YF; Ding, Y; Yang, ZL; Li, SB; Zhou, XS; Fan, FR; Zhang, W; Zhou, ZY; Wu, DY; Ren, B; Wang, ZL; Tian, ZQ, *Shell-Isolated Nanoparticle-Enhanced Raman Spectroscopy.* Nature, 2010. **464** (7287): p. 392-395.

75. Geddes, C.D.A., K.; Gryczynski, I.; Malicka, J.; Lakowicz, J. R. , Rev Fluoresc 2004. **1**: p. 365-401.

76. Aroca, R.F., et al., *Surface-enhanced Raman scattering on colloidal nanostructures.* Advances in Colloid and Interface Science, 2005. **116**(1-3): p. 45-61.

77. Kurt, M., et al., *Molecular structure, vibrational, UV and NBO analysis of 4-chloro-7-nitrobenzofurazan by DFT calculations.* Spectrochimica Acta Part a-Molecular and Biomolecular Spectroscopy, 2011. **79**(5): p. 1162-1170.

78. Lambert, J.B., et al., *Introduction to Organic Spectroscopy*1987, New York: Macmillan Publishing Company.

VITA AUCTORIS

NAME: **Aisha Alsaleh**

PLACE OF BIRTH: **Al-Hasa, Saudi Arabia**

YEAR OF BIRTH: **1987**

EDUCATION: **10th Secondary School, Dammam, Saudi Arabia**

2002-2005

King Faisal University, Dammam, Saudi Arabia

2006-2009